JOURNAL OF GEOPHYSICAL RESEARCH: BIOGEOSCIENCES, VOL. 118, 529–548, doi:10.1002/jgrg.20051, 2013

Characterization and intercomparison of global moderate resolution leaf area index (LAI) products: Analysis of climatologies and theoretical uncertainties

Hongliang Fang,[1] Chongya Jiang,[1] Wenjuan Li,[1] Shanshan Wei,[1] Frédéric Baret,[2] Jing M. Chen,[3] Javier Garcia-Haro,[4] Shunlin Liang,[5,6] Ronggao Liu,[7] Ranga B. Myneni,[8] Bernard Pinty,[9] Zhiqiang Xiao,[10] and Zaichun Zhu[8]

Received 26 December 2012; revised 14 March 2013; accepted 16 March 2013; published 17 April 2013.

[1] Leaf area index (LAI) is a critical variable for land surface and climate modeling studies. Several global LAI products exist, and it is important to know how these products perform and what their uncertainties are. Five major global LAI products—MODIS, GEOV1, GLASS, GLOBMAP, and JRC-TIP—were compared between 2003 and 2010 at a 0.01° spatial resolution and with a monthly time step. The daily Land-SAF product was used as a regional reference in order to evaluate the performance of other global products in Africa. Cross-sensor LAI conversion equations were derived for different biome types. Product uncertainties were assessed by looking into the product quantitative quality indicators (QQIs) attached to MODIS, GEOV1, and JRC-TIP. MODIS, GEOV1, GLASS, and GLOBMAP are generally consistent and show strong linear relationships between the products ($R^2 > 0.74$), with typical deviations of < 0.5 for nonforest and < 1.0 for forest biomes. JRC-TIP, the only effective LAI product, is about half the values of the other LAI products. The average uncertainties and relative uncertainties are in the following order: MODIS (0.17, 11.5%) < GEOV1 (0.24, 26.6%) < Land-SAF (0.36, 37.8%) < JRC-TIP (0.43, 114.3%). The highest relative uncertainties usually appear in ecological transition zones. More than 75% of MODIS, GEOV1, JRC-TIP, and Land-SAF pixels are within the absolute uncertainty requirements (± 0.5) set by the Global Climate Observing System (GCOS), whereas more than 78.5% of MODIS and 44.6% of GEOV1 pixels are within the threshold for relative uncertainty (20%). This study reveals the discrepancies mainly due to differences between definitions, retrieval algorithms, and input data. Future product development and validation studies should focus on areas (e.g., sparsely vegetated and savanna areas) and periods (e.g., winter time) with higher uncertainties.

Citation: Fang, H., et al. (2013), Characterization and intercomparison of global moderate resolution leaf area index (LAI) products: Analysis of climatologies and theoretical uncertainties, *J. Geophys. Res. Biogeosci.*, *118*, 529–548, doi:10.1002/jgrg.20051.

1. Introduction

[2] Leaf area index (LAI) indicates the area of live green leaves in the canopy per unit of ground surface. It is one of the essential climate variables defined by the Global Climate Observing System (GCOS) that are important in improving the parameterization of the land surface-atmosphere interaction processes in a range of models [*GCOS*, 2011]. Over the last decade, a number of LAI products with different spatial

[1]LREIS, Institute of Geographic Sciences and Natural Resources Research, Chinese Academy of Sciences, Beijing, China.
[2]INRA-EMMAH UMR 1114, Avignon, France.
[3]Department of Geography, University of Toronto, Toronto, Ontario, Canada.
[4]Departament de Física de la Terra i Termodinàmica, Facultat de Física, Universitat de València, Burjassot, Spain.

Corresponding author: H. Fang, LREIS, Institute of Geographic Sciences and Natural Resources Research, Chinese Academy of Sciences, Beijing 100101, China. (fanghl@lreis.ac.cn)

2169-8953/13/10.1002/jgrg.20051

[5]College of Global Change and Earth System Science, Beijing Normal University, Beijing, China.
[6]Department of Geographical Sciences, University of Maryland, College Park, Maryland, USA.
[7]Institute of Geographic Sciences and Natural Resources Research, Chinese Academy of Sciences, Beijing, China.
[8]Department of Earth and Environment, Boston University, Boston, Massachusetts, USA.
[9]Global Environment Monitoring Unit, Institute for Environment and Sustainability, DG Joint Research Centre, European Commission, Ispra, Italy.
[10]State Key Laboratory of Remote Sensing Science, School of Geography, Beijing Normal University, Beijing, China.

Table 1. Characteristics of MODIS, GEOV1, GLASS, GLOBMAP, JRC-TIP, and Land-SAF LAI Products

Products	Version	Spatial Resolution	Temporal Resolution	Algorithms	Lt/Le	Uncertainty Provided?	References
MODIS	MCD15 C5	1 km	8 day	LUT (red, NIR)	T	Yes	*Huang et al*. [2008]
GEOV1	V1.0	1/112°	10 day	NN (red, NIR, SWIR, SZA)	T	Yes	*Baret et al.* [2013]
GLASS	V3.0	1 km	8 day	NN (red, NIR)	T	No	*Xiao et al*. [2013]
GLOBMAP	V1.0	500 m	8 day	Empirical VI-LAI relationship	T	No	*Liu et al*. [2012]
JRC-TIP	V1.0	0.01°	16 day	Data assimilation retrieval from albedo	E	Yes	*Pinty et al*. [2011b]
Land-SAF	V2.0	3 km	Daily	Empirical fCover-LAI relationship	T	Yes	*García-Haro et al.* [2008]

"Lt/Le" refers to true (T)/effective (E) LAI. LUT, NIR, NN, SWIR, SZA, and VI stand for look-up table, near infrared, neural network method, shortwave infrared, solar zenith angle, and vegetation index, respectively.

and temporal characteristics have become available, for example, the 1 km MODIS products from the TERRA and AQUA platforms [*Huang et al*., 2008; *Myneni et al*., 2002], the 10 day CYCLOPES V3.1 LAI generated from the SPOT/VEGETATION sensor [*Baret et al*., 2007], and the monthly 1 km GLOBCARBON V2.0 LAI product derived from the combined use of the SPOT/VEGETATION and ENVISAT/ATSR instruments [*Deng et al*., 2006; *Plummer et al*., 2006]. More recently, several new global LAI products have appeared: GEOV1, GLASS, GLOBMAP, and JRC-TIP (Table 1). Other LAI products have been produced for a specific region, such as the Land-SAF LAI, obtained from MSG/SEVIRI, for Africa, Europe, and South America (Table 1).

[3] Characterization of uncertainties associated with LAI products is essential for the application community [*Gobron and Verstraete*, 2009; *Lafont et al*., 2012]. A better understanding of the uncertainties embedded in current LAI products will improve the assimilation of the LAI into land surface modeling studies [*Rüdiger et al*., 2010]. Various configurations of LAI uncertainties have been extensively investigated in the literature. LAI uncertainty can be easily represented by an overall constant value [*Sabater et al*., 2008]. However, several authors have proposed using different uncertainties for different LAI values [*Barbu et al*., 2011; *Pauwels et al*., 2007], e.g., 0.2, 0.4, and 0.6 for LAI values less than 1, 2, and 3, respectively. More frequently, the LAI uncertainty is set to an empirical percentage (e.g., 10% or 20%) of the LAI value [*Jarlan et al*., 2008; *Rüdiger et al*., 2010]. In order to meet the needs of global climate modeling studies, GCOS has proposed a guideline which requires an accuracy of ±0.5 for the LAI products [*GCOS*, 2011]. Furthermore, the LAI application communities require a minimum relative accuracy of about 20% (Table 2).

[4] Product uncertainty information can be categorized into two types: theoretical and physical [*Fang et al*., 2012c]. Theoretical uncertainties are caused by uncertainties in the input data, model imperfections, and the inversion process and are usually estimated and reported using quantitative quality indicators [*Baret et al*., 2007; *Knyazikhin et al*., 1999; *Pinty et al*., 2011b]. Theoretical uncertainties can also be derived using uncertainty estimation tools, such as the triple collocation error model [*Fang et al*., 2012c]. Physical uncertainties are derived through comparison with values representing the ground truth, such as field measurements or estimations from higher-resolution imagery. In practice, both theoretical and physical uncertainties have been used as product quality indicators [*GCOS*, 2011].

[5] To better understand the consistency of existing LAI products and their associated uncertainties, a series of systematic validation and intercomparison studies have been carried out by the Committee on Earth Observation Satellites (CEOS) Land Product Validation (LPV) subgroup (http://lpvs.gsfc.nasa.gov/). These studies have been undertaken for either a fixed number of sites [*Abuelgasim et al*., 2006; *De Kauwe et al*., 2011; *Kobayashi et al*., 2007; *Pisek and Chen*, 2007] or globally [*Fang et al*., 2012a; *Garrigues et al*., 2008; *Verger et al*., 2009; *Weiss et al*., 2007]. The intercomparison approach requires no ground measurement and determines the quality of one product relative to the quality of other products [*Morisette et al*., 2006]. The approach has been used to assess temporal consistency and spatial and statistical distributions within and between sensors [*Camacho et al*., 2010; *Fang et al*., 2012a, 2012b, 2012c; *Garrigues et al*., 2008; *Verger et al*., 2009; *Weiss et al*., 2007]. However, further intercomparison studies using products that are closest to the native spatial and temporal resolution of the sensors (i.e., ~1 km in this study) are needed in order to investigate the interannual variability of vegetation [*Gobron and Verstraete*, 2009].

Table 2. Observational Accuracy Requirements for LAI Products From GCOS, GTOS, WMO and GMES[a]

Projects	Application	Accuracy Requirement[b]	References
GCOS	TOPC	10%−7%−5%	*GCOS* [2007]
		0.5	*GCOS* [2011]
GTOS		25%−15%	GTOS[c]
WMO	Agricultural meteorology	10%−6.3%−5%	*WMO* [2011]
	Global NWP	20%−10%−5%	
	High resolution NWP	10%−5%−3%	
	Hydrology	20%−7.9%−5%	
GMES		10%	*Drusch et al.* [2010]

[a]GCOS: Global Climate Observing System; GTOS: Global Terrestrial Observing System; WMO: World Meteorological Organization; GMES: Global Monitoring for Environment and Security; NWP: Numerical Weather Prediction; TOPC: Terrestrial Observation Panel for Climate.

Accuracy requirements are denoted as a percentage of the maximum possible value for GCOS and as a percentage of the true value for GTOS and WMO.

[b]Stated in terms of the minimum, the breakthrough, and the targeted values. The GMES row shows the targeted precision for green LAI estimation.

[c]GTOS web site—http://www.fao.org/gtos/tems/variable_show.jsp?VARIABLE_ID=80 (accessed on 1 March 2012).

[6] Understanding and quantifying the quality of the LAI products are challenging tasks for the remote sensing community [*Fang et al*., 2012a, 2012c]. Currently, LAI values are usually distributed along with the quality information, either qualitative or quantitative, in order to show the product processing status and the quality information. Qualitative quality flags (QQFs) have been taken into account by most validation studies [e.g., *Abuelgasim et al*., 2006; *Garrigues et al*., 2008; *Kobayashi et al*., 2007; *Pisek and Chen*, 2007; *Sprintsin et al*., 2009; *Weiss et al*., 2007]. However, as far as can be ascertained, no study has systematically investigated the quantitative quality indicators (QQIs) at a global level. The QQFs are categorical and cannot be used to describe the uncertainties at a pixel level. The QQIs, distributed along with the LAI products, are quantitative and provide the information about the LAI product features and their uncertainties. An assessment of these quantitative indicators is thus critical if the spatial and temporal patterns of global LAI uncertainties are to be understood.

[7] The objective of this study is to provide an intercomparison of current global LAI products so that their characterizations and uncertainties can be better understood. This study extends an earlier intercomparison study of the MODIS, CYCLOPES, and GLOBCARBON products [*Fang et al*., 2012b]. A new suite of five major global LAI products—MODIS, GEOV1, GLASS, GLOBMAP, and JRC-TIP—was examined and compared in order to characterize the global LAI seasonality and quality variation. The continental Land-SAF product was used as a reference in order to assess the performances of other global products in Africa. These products span the full spectrum of different satellite sensors, LAI estimation algorithms, and uncertainty representations, and the product details can be easily found from various reference sources. Special attention has been paid to the product quality indicators in order to investigate the uncertainties and relative uncertainties of the products. This study intends to answer several crucial questions as follows: (1) How do the products compare with each other, in terms of LAI values, theoretical uncertainties and relative uncertainties? (2) What is the best method for making conversions between the products where there are missing values? (3) How have the current products improved compared to their earlier versions? (4) How do the current products, based on their own quality indicators, compare with the quality requirement proposed by GCOS?

2. Data Sets and Methods

2.1. MODIS LAI Product

[8] The MODIS collection 5 product, acquired from the combined TERRA and AQUA platforms (MCD15A2), is generated every 8 days in a 1 km spatial resolution (http://wist.echo.nasa.gov, accessed on 1 March 2012). The product uses eight biome types as a priori information to constrain the vegetation optical and structural parameter spaces: (1) grasses/cereal crops, (2) shrubs, (3) broadleaf crops, (4) savanna, (5) evergreen broadleaf forest (EBF), (6) deciduous broadleaf forest (DBF), (7) evergreen needleleaf forest (ENF), and (8) deciduous needleleaf forest (DNF) [*Yang et al*., 2006]. The main algorithm employs a look-up table (LUT) method simulated from a 3-D radiative transfer model [*Knyazikhin et al*., 1998a, 1998b]. In collection 5, a stochastic radiative transfer equation is applied [*Huang et al*., 2008]. The LUT method essentially searches for LAIs for a specific set of solar and view zenith angles, observed bidirectional reflectance factors (BRFs) at certain spectral bands and biome types. The outputs are the LAI mean values averaged over all acceptable solutions, and the standard deviation (LaiStdDev) serving as a measure of the solution accuracy. The LaiStdDev has been released to the public as part of the collection 5 data. A quality control mask indicates whether the LAI value is derived from the main method or from the empirical backup method.

2.2. GEOV1 LAI Product

[9] The Geoland2 project (http://www.gmes-geoland.info) aims to implement the GMES (Global Monitoring for Environment and Security) Land Monitoring Services, which represents to the European contribution to GEOSS (Group of Earth Observation System of Systems). One component of the project, Geoland2/BioPar, has developed the first version of a global biophysical product, GEOV1, from the SPOT/VEGETATION observations at 1/112° (about 1 km at the equator) spatial resolution with a 10 day time step in a Plate Carrée projection (http://www.geoland2.eu). The MODIS and CYCLOPES products are first fused to generate "best estimates" of the LAIs that are then scaled to closely match their expected range of variation [*Baret et al.*, 2013]:

$$LAI_{\text{fused}} = w \cdot LAI_{\text{MOD}} + (1 - w) \cdot LAI_{\text{CYC}}, \quad \text{with}$$
$$w = \min\left(1, \tfrac{1}{4} LAI_{\text{CYC}}\right) \tag{1}$$

where the subscripts "fused," "MOD," and "CYC" correspond to the fused, MODIS, and CYCLOPES products, respectively. The weight, w, is driven by LAI_{CYC} since it appears more stable at low LAI values compared to MODIS. The threshold value: $\text{LAI}_{\text{CYC}} = 4$, corresponds to the value when LAI_{CYC} starts to saturate. A neural network training process is performed between the fused LAI and the SPOT/VEGETATION top of canopy directionally normalized reflectance values at the global BELMANIP sites [*Baret et al*., 2006]. Once the neural network is calibrated, it is run to provide LAI estimates from the SPOT/VEGETATION sensor, along with the quality flags and quantitative uncertainties. Clumping effects at the landscape level have been accounted for in CYCLOPES through the separation of pure vegetation and bare soil in a pixel [*Baret et al*., 2007]. The quantitative uncertainties (LAI_ERR) are computed using the training dataset and reflect the sensitivity of the product to input reflectance values [*Baret et al.*, 2013]).

2.3. GLASS LAI Product

[10] The Global Land Surface Satellite (GLASS) project estimates LAIs from MODIS and AVHRR time series reflectance data using a neural network approach [*Xiao et al*., 2013]. The 8 day, 1 km GLASS LAI product (version 3.0) is available from the Beijing Normal University (BNU) (http://www.bnu-datacenter.com/) in the Integerized Sinusoidal (ISIN) projection. The "effective" CYCLOPES

LAI (LAI_e) is converted to the true value (LAI_t) using the following formula:

$$LAI_t = LAI_e/\Omega \quad (2)$$

where Ω is the clumping index derived from POLDER [*Chen et al*., 2005]. After transformation, the MODIS LAI and CYCLOPES LAI_t are combined in a weighted linear combination in order to obtain the best LAI estimate. In contrast to GEOV1 (equation (1)), GLASS uses the spatiotemporally varied weights determined by MODIS and CYCLOPES for each biome type:

$$LAI_{fused} = w \cdot LAI_{MOD} + (1 - w) \cdot LAI_{CYC\_t}, \quad (3)$$

where the subscripts "fused," "MOD," and "CYC_t" correspond to the fused, MODIS, and converted CYCLOPES LAI values, respectively. Linear regressions are constructed between MODIS and CYCLOPES LAIs and the ground values for each biome type. The weight, w, is determined by the deviation of MODIS and CYCLOPES from the ground LAI [*Xiao et al*., 2013]. The MODIS red and near-infrared reflectance data (MOD09A1) are reprocessed to remove cloud contaminated data and to fill in missing values using temporal-spatial filtering algorithms [*Tang et al*., 2013]. A general regression neural network (GRNN) is trained for each biome type using the combined LAI and the reprocessed MODIS reflectance values over the BELMANIP sites [*Baret et al*., 2006] between 2001 and 2003. The trained GRNNs are used to estimate LAIs from the yearly reprocessed MODIS reflectance data [*Xiao et al*., 2013]. A quality control layer is attached to GLASS LAIs to show the processing status, the quality of the input reflectance and the contamination by snow, cloud, and shadow.

2.4. GLOBMAP LAI Product

[11] The GLOBMAP project derives global LAI (1981–2011) by quantitatively fusing the MODIS and AVHRR observations [*Liu et al*., 2012]. The effective LAI is first generated from MODIS land surface reflectance data (MOD09A1) based on the GLOBCARBON LAI algorithm [*Deng et al*., 2006]. The GLOBCARBON algorithm relies on land cover-specific LAI-vegetation index relationships simulated from a four-scale geometrical optical model [*Chen and Leblanc*, 1997; *Deng et al*., 2006]. The IGBP land classes are grouped into six biomes (crops/grasses and others, conifer, tropical, deciduous, mixed forest, and shrub) and one nonvegetated class [*Deng et al*., 2006]. The GLOBMAP effective LAI is then converted to the true LAI using the 500 m global clumping index data [*He et al*., 2012]. Pixel level relationships are established between the true LAI and vegetation indices for AVHRR and MODIS during their overlapping period. The relationships are then utilized to estimate long-term pixel level LAI for both AVHRR and MODIS over the non-overlapping periods. This study used the global 8 day, 500 m LAI series retrieved from the MODIS observations (http://www.globalmapping.org/globalLAI, version 1.0).

2.5. JRC-TIP LAI Product

[12] JRC-TIP is the only effective LAI product explored in this study. The 16 day, 0.01° LAI product is generated at the Joint Research Centre (JRC) to help bridge the gap between remote sensing products and large-scale global climate models [*Pinty et al*., 2011b]. The inversion algorithm, called the Two-stream Inversion Package (JRC-TIP) [*Pinty et al*., 2006], uses the white sky albedo product, derived from MODIS and MISR in the visible and near-infrared (NIR) domains, to infer the probability density functions (PDFs) of the effective LAI. The methodology uses automatic differentiation techniques to generate the adjoint and Hessian codes of a cost function [*Pinty et al*., 2011b]. The retrieval uncertainties (Xstd) are the standard deviations relating to the diagonal of the posterior covariance matrix and denote the monthly dispersion of LAI values. The uncertainties are derived from prior PDFs and observations and model uncertainties.

2.6. Land-SAF LAI Product

[13] The Land-SAF LAI version 2.0 is generated daily at a 3 km spatial resolution from the MSG/SEVIRI instrument over four specific geographical regions under the MSG disk (Europe, North Africa, South Africa, and South America) (http://landsaf.meteo.pt/). The LAI is estimated using a semi-empirical exponential relationship with the fractional vegetation cover (FVC) [*Roujean and Lacaze*, 2002]. Three SEVIRI short-wave channels (visible, near-infrared, and shortwave infrared) are used as inputs for deriving the FVC product. The LAI product is thus obtained directly from the cloud-free FVC product, which has been corrected for view/sun angles and anisotropy effects. The algorithm incorporates a biome-dependent clumping index to correct for the clumping effect on LAI estimates [*Chen et al*., 2005]. The overall LAI error depends primarily on the input FVC error. Details about the algorithm, implementation, and validation have been documented in *García-Haro et al*. [2008]

2.7. Data Analysis

[14] This study analyzed the five global LAI products between 2003 and 2010 to characterize their performances. Global pixel level uncertainties provided by MODIS, GEOV1, and JRC-TIP products were analyzed. All global tiles were first mosaicked and then resampled to a 0.01° spatial resolution using the nearest neighbor resampling method on the Plate Carée projection. Because each data set has a different temporal compositing period, the data sets and their quantitative quality indicators (QQIs) were aggregated into a monthly time step using the averaging method, which enabled direct comparisons of the products. This paper refers to the QQIs distributed in the standard LAI products as the product uncertainties. The relative uncertainty was calculated as the ratio of the uncertainty divided by the LAI values. Raw LAI data that had been corrupted or had missing geometry information (flagged with filled values) were excluded from the aggregation. Only MODIS pixels retrieved from the main algorithms were considered in the composition. For the JRC-TIP products, only pixels where the quality flags are all "OK" (majority of the cases) were considered.

[15] For consistency purposes, this study used the MODIS biome type map (2003) provided in the 0.05° MODIS/Terra + Aqua collection 5 land cover type product (MCD12C1) [*Friedl et al*., 2010], as a base map for LAI products analysis. For the sake of computation efficiency

and compatibility with the biome map, LAI climatologies and uncertainties were analyzed over the whole globe using 0.05° grid cells. The correlations between each pair of LAI products were examined in order to derive translation equations that would allow missing LAI products, due to retrieval failure or lack of satellite coverage for a given long-term LAI time series, to be filled in [*GCOS*, 2011].

[16] A continental intercomparison was performed in accordance with the Land-SAF coverage in order to explore the temporal and spatial consistency of LAIs and uncertainties in Africa (2007−2010). This study did not separate the two hemispheres in the calculation as the main aim is to make an intercomparison between different products. In order to understand how well the products perform compared to the earlier releases, the present GEOV1 and GLOBMAP products were compared to their heritage products: CYCLOPES V3.1 and GLOBCARBON V2.0, respectively. Since the uncertainty information is not available for GLASS and GLOBMAP, theoretical uncertainties were evaluated for the other four products in order to assess their conformity with user requirements (Table 2). It should be noted that the theoretical uncertainties explored in this study generally resemble the random errors, whereas the GCOS requirements for physical uncertainties represent the systematic errors.

3. Results

3.1. Intercomparison of Global LAI Products

3.1.1. Spatial Consistency of Global LAI Products

[17] Figure 1 shows the geographical distribution of global average LAIs from 2003 to 2010. MODIS, GEOV1, GLASS, and GLOBMAP LAI products are generally consistent in their spatial patterns and are in agreement with regard to their magnitudes. The general consistency is associated with the fact that all the products represent the true LAI, even if their retrieval algorithms and reflectance data sources differ from one another. The two hemispheres clearly show opposite seasonality. There are three clear LAI peaks in the northern hemisphere, which are located in the tropical (0°N), subtropical (20°N), and boreal regions (60°N). The equatorial regions, e.g., Amazonia and central Africa, have the highest LAIs (> 5.0), followed by the boreal areas, which is in accordance with the forest distribution. The LAI values are intermediate at middle latitudes and are associated with agricultural activities and broadleaf forests, for example, over the United States, Europe, and China. The LAI values are very low (< 1.0) over sparsely vegetated areas. Missing LAI values (white areas in Figure 1) can be easily seen in the desert regions and during the winter and are caused by the lack of quality input data. MODIS and GLASS are very similar, and both show the highest LAIs (4.3) in the tropical regions. GEOV1 and GLOBMAP values are slightly lower (~0.5) in the tropical regions compared to the MODIS and GLASS values. GLOBMAP values are also lower (~0.6) than the other true LAI products in the subtropical regions. All products show small LAI peaks (~1.5) and high variability around 40°S−50°S. The JRC-TIP (effective) LAIs clearly produce the lowest values (< 1.5) at a global scale and are, on average, about one third of values calculated by the other products.

3.1.2. Global LAI Climatologies

[18] Figure 2 shows the climatologies of all LAI products from 2003 to 2010. All the products generally show a smooth seasonal evolution with higher values in summer and lower in winter. All the climatologies agree very well for grasses/cereal crops and shrubs, with mean deviations of less than 0.33 (Table 3). Small differences (< 0.85) are recorded for broadleaf crops and savanna. For broadleaf crops, GEOV1 and GLASS values are slightly higher (~0.25) than the MODIS values, while the GLOBMAP and JRC-TIP values are lower (~0.20) than the MODIS values. For savanna, the MODIS, GEOV1, and GLASS values are similar, but the GLOBMAP and JRC-TIP values are lower (~0.45) than the MODIS values.

[19] MODIS, GEOV1, GLASS, and GLOBMAP produce relatively stable LAIs for EBF over the year. MODIS and GLASS overestimate GEOV1 and GLOBMAP by about 0.50. Possible reasons are discussed in section 4.1. All of the four true LAI products produce similar values for DBF, ENF, and DNF. GEOV1 produce slightly higher values for needleleaf forests in winter, especially for DNF, which is partly due to snow and cloud contamination. Overestimation also occurs in the earlier CYCLOPES product and will be further discussed in section 3.5. For JRC-TIP, the effective LAI values are about half of the other true LAI products on average (Table 3). The underestimation is less pronounced for herbaceous types, for which the JRC-TIP temporal profiles are similar to those of GLOBMAP. The underestimation is more pronounced for forest types during the maturity stage, reaching 4.0 for EBF. The LAI values for the nonvegetated areas are, understandably, low (< 0.30). The urban pixels make up a small percentage of the data and display a clear seasonal variation.

3.1.3. Relationships and Conversions Between LAI Products

[20] Figure 3 shows the density scatter plots between the global LAI products. The MODIS, GEOV1, GLASS, and GLOBMAP LAI products show strong linear correlations with one another, with R^2 values ranging between 0.743 and 0.896. Although the data points are scattered, the correlation between GEOV1 and MODIS is as high at $R^2 = 0.789$, and they differ by only 0.38 LAI (Figure 3a). Both MODIS and GEOV1 become saturated at about 6.0, due to the fact that the fused GEOV1 is mainly driven by MODIS for larger LAI values. The excellent agreement between MODIS and GEOV1 indicates that after taking into account the fusion equation (1), the GEOV1 LAI is close to the MODIS true LAI. GLASS shows the highest correlation with MODIS ($R^2 = 0.855$) and GEOV1 ($R^2 = 0.896$). The good consistency between MODIS, GEOV1, and GLASS is expected because the fusion algorithm makes use of the best LAI estimates (equations (1) and (3)) in the neural network training process, which smoothes out possible outliers contaminated by clouds, snow, or atmospheric effects and provides improved consistency between products. GLOBMAP produces a small number of rather high LAI values (> 7.0; Figures 3d−3f), which correspond to EBF in southern Amazonia and is related to the fairly low pixel-level clumping index (0.5−0.6) data [*He et al.*, 2012; *Liu et al.*, 2012]. The graphics for JRC-TIP are different from those of the other scatter plots (Figures 3g−3j). JRC-TIP values are about one third of the other LAI values and have a low

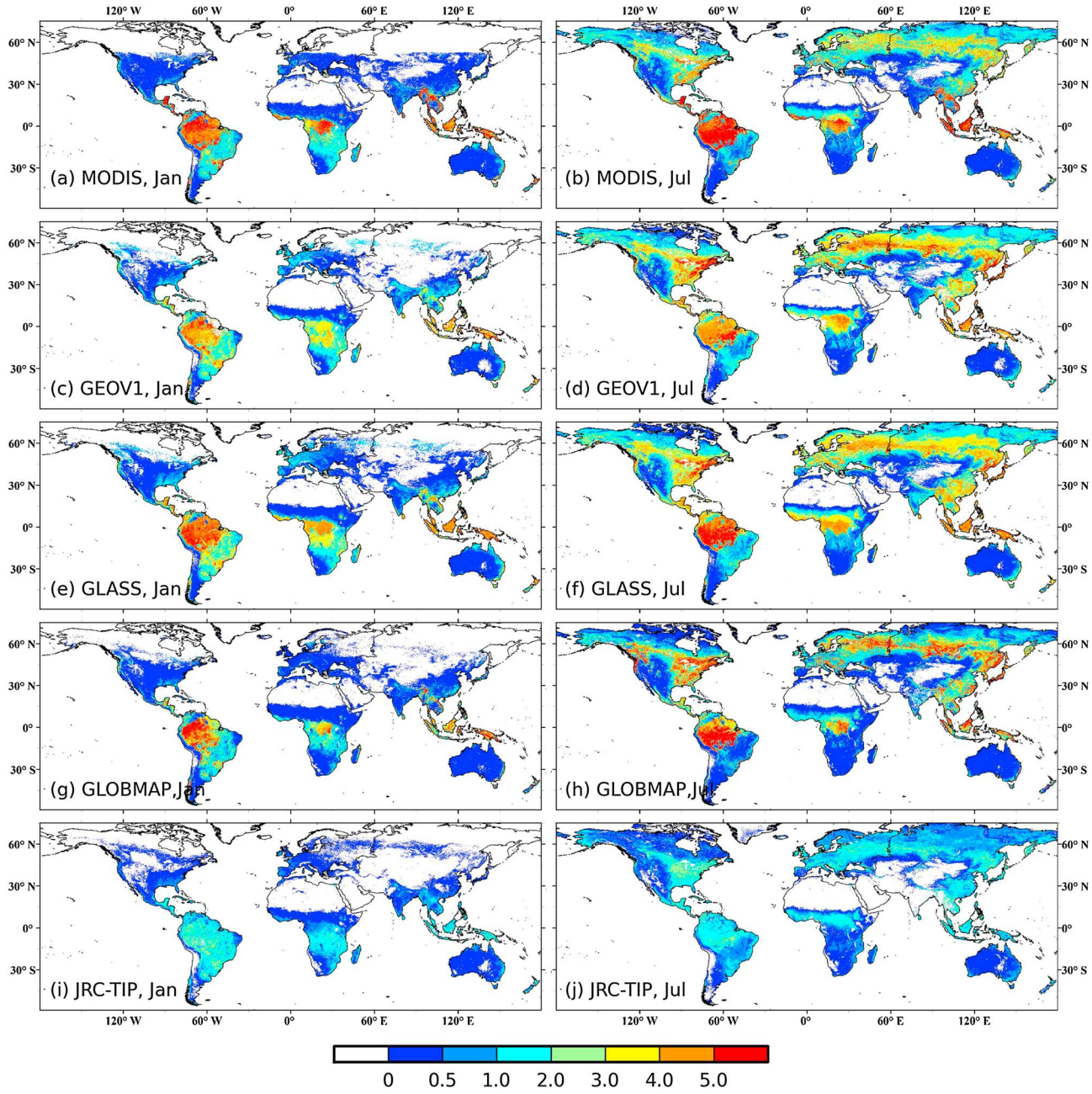

Figure 1. Global mean LAI from MODIS, GEOV1, GLASS, GLOBMAP, and JRC-TIP from 2003 to 2010 (0.05°) in January (left panels) and July (right panels), respectively.

relationship ($R^2 \leq 0.661$) with these products. The effective LAI generally saturates at 3.0 or slightly higher, which represents an upper boundary for JRC-TIP retrievals with regard to prior values and observational uncertainties [*Pinty et al.*, 2011b].

[21] Table 4 gives the conversion equations between the LAI products for different biome types. The MODIS LAI was used as a baseline because GEOV1, GLASS, GLOBMAP, and JRC-TIP are, to some extent, connected to MODIS in the LAI retrieval process. The linear function performs well in translating the LAI values among the different products, although some variability exists. Good relationships are found for grasses/cereal crops, shrubs, DBF, ENF, and DNF. The moderate relationships ($R^2 \leq 0.60$) for broadleaf crops are due to overestimations (~1.0−2.0) by GEOV1, GLASS, and GLOBMAP in the Midwestern United States corn and soybean belt and underestimations (~2.0) in the tropical West Africa in summer (Figure 1). The similarly moderate relationships for savanna reveal differences between the products for this structurally complicated biome type [*Fang et al.*, 2013]. The low relationships ($R^2 < 0.42$) for evergreen broadleaf forest can be partly attributed to the small range of high values for this particular biome type, even though the mean deviations among the products are less than 0.50 (Figure 2).

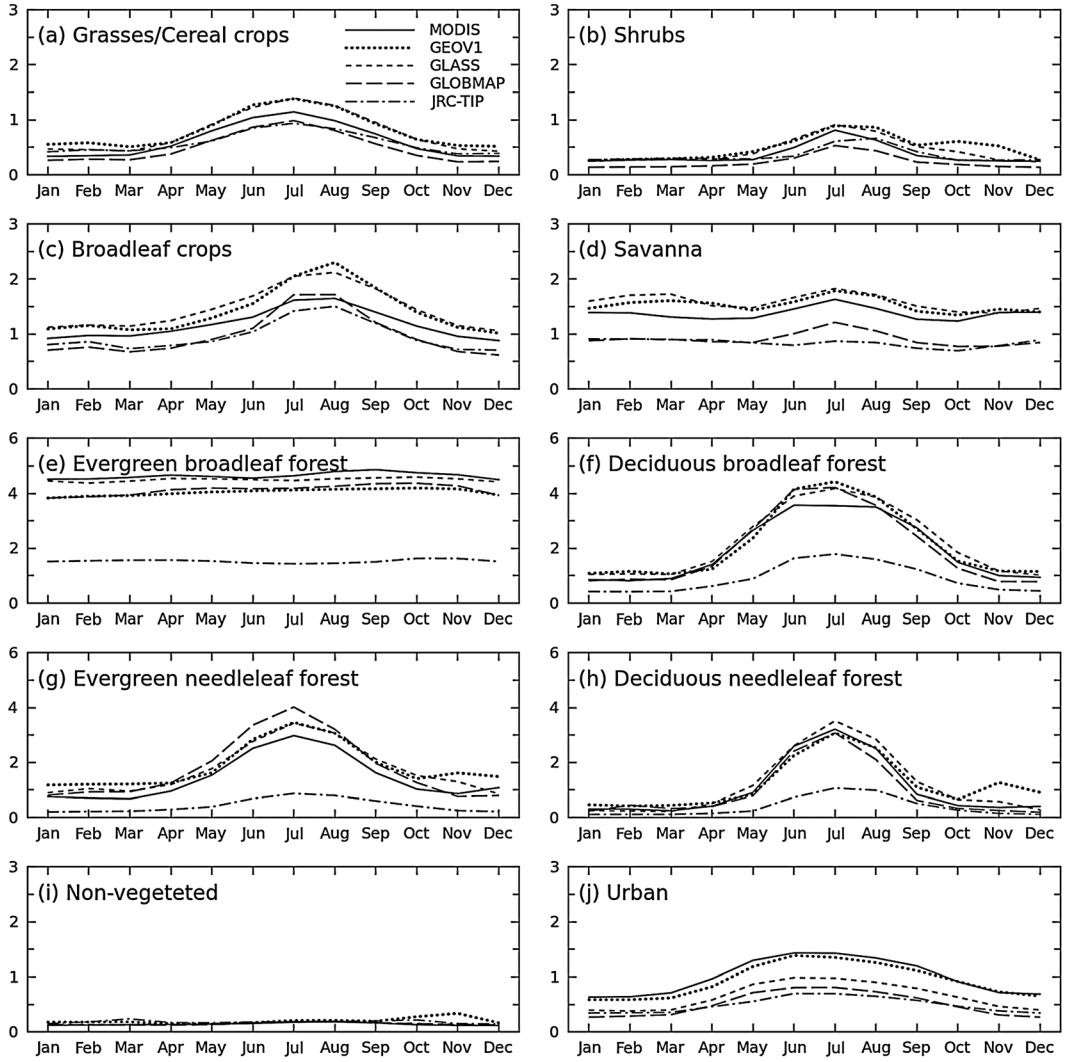

Figure 2. Climatologies of global monthly MODIS, GEOV1, GLASS, GLOBMAP, and JRC-TIP LAI products for different biome types from 2003 to 2010 (0.05°).

Table 3. Yearly Mean LAI, Uncertainties, and Relative Uncertainties for Different Biome Types, 2003–2010[a]

	Biome Types	Grass/Crop-C	Shrub	Crop-B	Savanna	EBF	DBF	ENF	DNF	Non-V	Urban	Average
Mean LAI	MODIS	0.64	0.41	1.17	1.38	4.64	2.04	1.58	1.34	0.14	1.01	1.43
	GEOV1	0.84	0.57	1.42	1.53	4.05	2.27	2.03	1.55	0.20	0.94	1.55
	GLASS	0.79	0.51	1.46	1.58	4.50	2.28	1.91	1.54	0.15	0.65	1.55
	GLOBMAP	0.51	0.27	0.98	0.92	4.13	2.07	1.95	1.30	0.15	0.51	1.23
	JRC-TIP	0.61	0.41	0.96	0.83	1.53	0.92	0.46	0.53	0.19	0.50	0.78
	Land-SAF	0.78	0.54	1.46	1.67	3.46	2.31	2.03		0.31	1.26	1.63
Uncertainty	MODIS	0.07	0.05	0.09	0.16	0.38	0.36	0.43	0.33	0.02	0.12	0.17
	GEOV1	0.17	0.13	0.26	0.31	0.66	0.41	0.36	0.33	0.00	0.22	0.24
	JRC-TIP	0.40	0.24	0.69	0.62	1.14	0.62	0.42	0.39	0.01	0.44	0.43
	Land-SAF	0.25	0.21	0.36	0.47	0.88	0.54	0.43		0.2	0.3	0.36
Relative uncertainty (%)	MODIS	9.1	11.8	6.5	11.0	8.8	15.8	23.9	19.0	4.8	3.8	11.5
	GEOV1	33.8	35.1	24.6	23.5	15.9	23.3	18.4	25.9	6.2	29.3	26.6
	JRC-TIP	126.7	133.9	101.0	103.9	78.9	103.3	137.2	141.3	104.0	130.7	114.3
	Land-SAF	56.8	57.2	37.4	30.3	25.2	25.4	30.1		102.3	32.1	37.8

[a]Land-SAF derived from 2007 to 2010 over Africa. The last column is calculated from the global average of all vegetated pixels. Crop-C and Crop-B refer to the cereal crops and broadleaf crops, respectively. EBF, DBF, ENF, and DNF stand for the evergreen broadleaf forest, deciduous broadleaf forest, evergreen needleleaf forest, and deciduous needleleaf forest, respectively. Non-V indicates the non-vegetated type. In all statistics, positive (>0) values were considered for LAI, and non-negative (≥0) values for uncertainty and relative uncertainty.

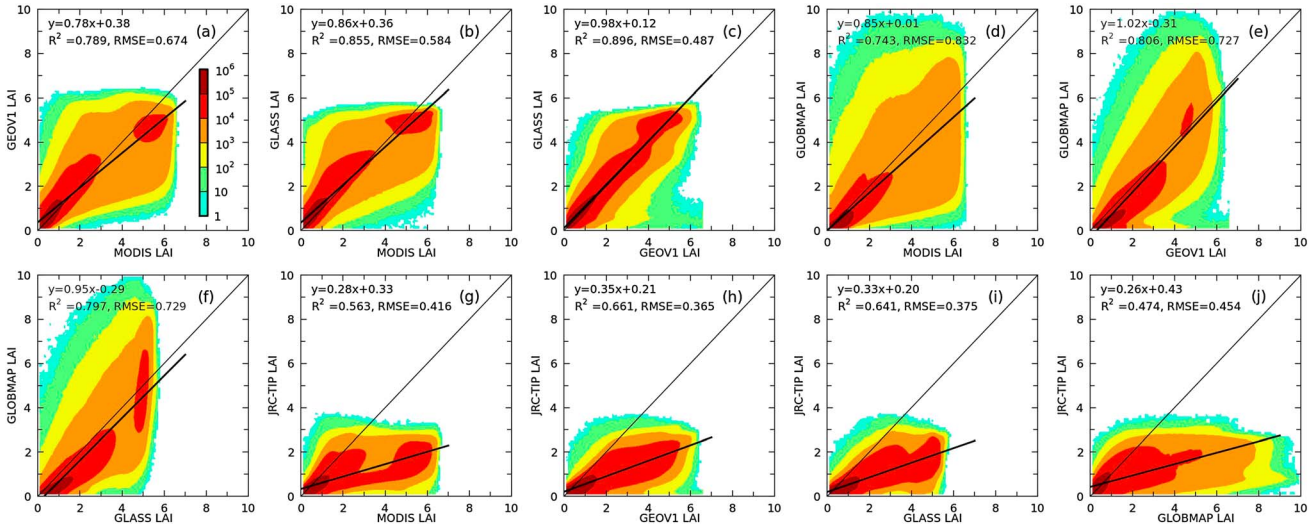

Figure 3. Density scatter plots between MODIS, GEOV1, GLASS, GLOBMAP, and JRC-TIP global LAI products from 2003 to 2010 (0.05°).

3.2. Theoretical Uncertainties of LAI Products

3.2.1. Spatial Consistency of LAI Uncertainties

[22] The uncertainty maps for MODIS, GEOV1, and JRC-TIP are presented in Figure 4. In general, the spatial patterns for the uncertainties are similar, correlate well with the distribution of biome types, and show that the tropical (20°S−15°N) and boreal regions (60°N) have higher uncertainties than the other areas. The overall uncertainties are generally in the following order: MODIS < GEOV1 < JRC-TIP. This trend is more obvious at lower latitudes. The MODIS uncertainty varies between 0.10 and 0.35 in the tropical regions, whereas the GEOV1 uncertainty is > 0.40 between 10°N and 10°S. JRC-TIP produces the highest uncertainty (~1.00) in the tropical regions. LAI uncertainties are also high in the boreal regions, which reflects the complex landscape caused by poor illumination, low solar zenith angle (SZA), snow and cloud contamination, and the understory effect [*Pisek et al.*, 2010; *Weiss et al.*, 2007]. The amplitudes of seasonal variability are visually correlated with the LAI products, with generally higher uncertainty in July than in January, except for the tropical regions. Data gaps are mostly caused by the occurrence of snow and cloud, especially in January. In July, higher GEOV1 uncertainties, compared to MODIS, are observed in eastern North America, Europe, and East Asia. For JRC-TIP, the uncertainties are also higher for forest and high LAI regions, for example, in the eastern United States and China. Moreover, the dynamic ranges of the uncertainties for JRC-TIP are considerably higher than those of MODIS and GEOV1, which reflects the higher monthly variation in the LAI data retrieved by MODIS albedo (section 2.5).

3.2.2. Temporal Variation in LAI Uncertainties

[23] The temporal variation in LAI uncertainties for MODIS, GEOV1, and JRC-TIP are compared in Figure 5. Seasonally, the product uncertainties are relatively higher in

Table 4. Translation Equations for Different LAI Products (y) as a Function of the MODIS LAI (x) for Different Biome Types[a]

Biome Types	GEOV1 ~ MODIS	GLASS ~ MODIS	GLOBMAP ~ MODIS	JRC-TIP ~ MODIS
Grass/ Cereal crops	$y=0.96x+0.16$ (0.736, 0.458)	$y=0.96x+0.18$ (0.777, 0.397)	$y=0.79x-0.00$ (0.759, 0.347)	$y=0.55x+0.18$ (0.675, 0.313)
Shrubs	$y=1.04x+0.09$ (0.736, 0.291)	$y=1.06x+0.09$ (0.773, 0.257)	$y=0.71x-0.02$ (0.753, 0.183)	$y=0.53x+0.15$ (0.630, 0.199)
Broadleaf crops	$y=0.63x+0.69$ (0.508, 0.750)	$y=0.66x+0.69$ (0.605, 0.662)	$y=0.53x+0.36$ (0.450, 0.726)	$y=0.36x+0.51$ (0.411, 0.539)
Savanna	$y=0.72x+0.51$ (0.572, 0.679)	$y=0.70x+0.62$ (0.636, 0.581)	$y=0.60x+0.09$ (0.600, 0.535)	$y=0.34x+0.36$ (0.458, 0.400)
Evergreen broadleaf forest	$y=0.41x+2.09$ (0.261, 0.887)	$y=0.41x+2.59$ (0.418, 0.645)	$y=0.61x+1.32$ (0.219, 1.522)	$y=0.21x+0.53$ (0.213, 0.519)
Deciduous broadleaf forest	$y=0.86x+0.49$ (0.702, 0.910)	$y=0.82x+0.65$ (0.766, 0.744)	$y=0.93x+0.19$ (0.698, 1.004)	$y=0.34x+0.25$ (0.644, 0.413)
Evergreen needleleaf forest	$y=0.83x+0.62$ (0.696, 0.625)	$y=0.81x+0.67$ (0.746, 0.539)	$y=1.13x+0.26$ (0.592, 1.069)	$y=0.23x+0.13$ (0.566, 0.231)
Deciduous needleleaf forest	$y=0.76x+0.37$ (0.780, 0.520)	$y=0.86x+0.42$ (0.823, 0.505)	$y=0.91x-0.02$ (0.796, 0.584)	$y=0.26x+0.16$ (0.606, 0.268)

[a]Equations derived from positive (>0) LAI values, 2003–2010 (0.05°). Each cell shows the conversion equations ($p < 0.001$), and R^2 and RMSE values in the brackets.

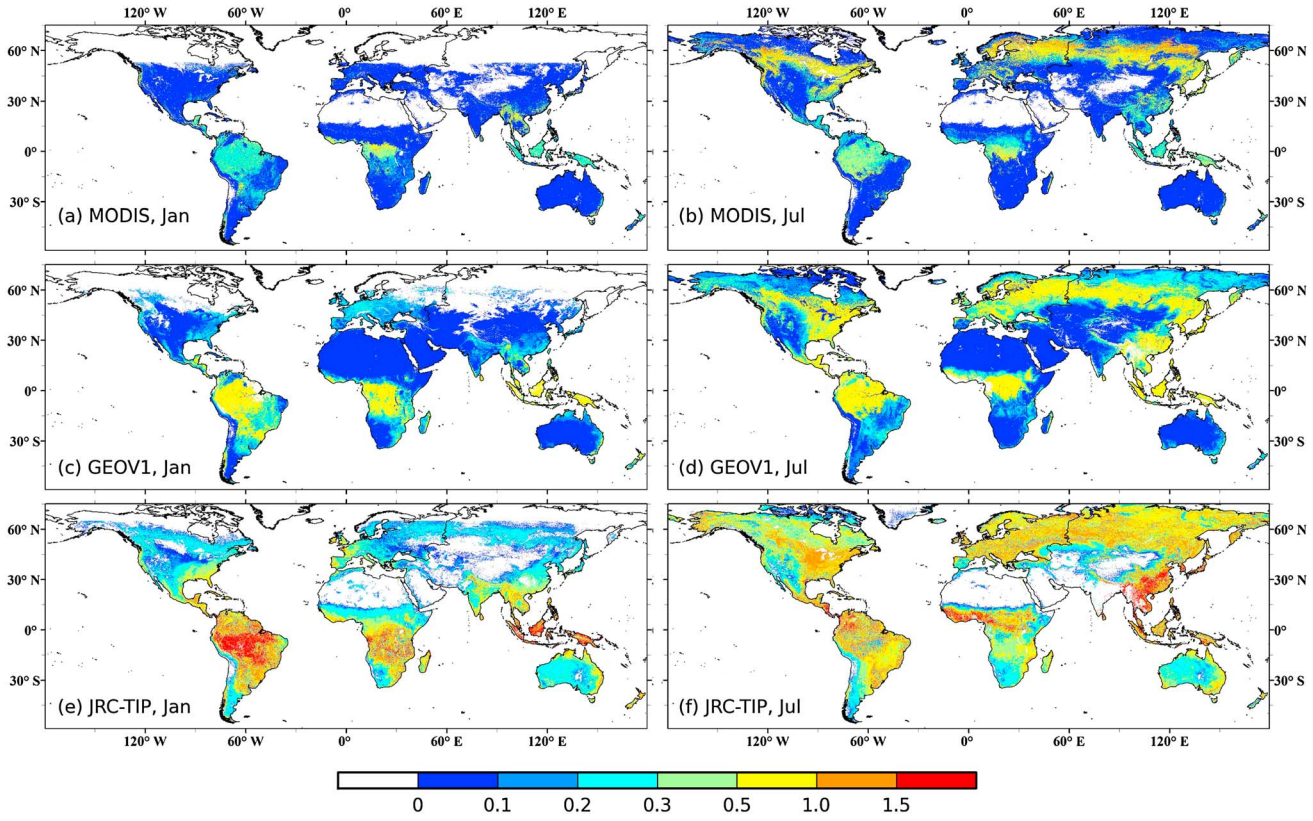

Figure 4. LAI uncertainty maps for MODIS, GEOV1, and JRC-TIP from 2003 to 2010 (0.05°) in January (left panels) and July (right panels), respectively.

summer and lower in winter. Similarly, the magnitude of the differences between the different products is normally higher in summer than in winter. Overall, MODIS and GEOV1 achieve similarly low uncertainties (0.17 versus 0.24). JRC-TIP uncertainty shows a clear seasonal pattern for all biome types. On average, the JRC-TIP uncertainty (0.43) is approximately twice the MODIS and GEOV1 uncertainties (Table 3).

[24] When individual biome types are considered, the uncertainties are generally in the order of MODIS < GEOV1 < JRC-TIP for grasses/cereal crops, shrubs, broadleaf crops, and savanna. MODIS and GEOV1 uncertainties are fairly stable and at a low level (< 0.30) over the year for these biome types, which is related to the low LAI values. For JRC-TIP, the uncertainty reaches about 0.96 for broadleaf crops in August. The uncertainties for forests are generally higher than those for nonforests (Figure 5). The highest uncertainty is observed for EBF, which is partly related to the high LAI values for the biome type (see more explanations in section 3.3.2). The uncertainties for MODIS (~0.38) and GEOV1 (~0.66) are stable over the year. In contrast, the JRC-TIP uncertainties are higher in spring (~1.44) than in summer (~0.99). MODIS and GEOV1 show similar uncertainties for DBF, ENF, and DNF, with average differences smaller than 0.1 (Table 3). MODIS, GEOV1, and JRC-TIP all display similar temporal variations for the three forest biome types, with larger uncertainties in summer than in winter. For DBF, the JRC-TIP uncertainty is slightly higher (~0.20) than the MODIS and GEOV1 uncertainties.

3.3. Relative Uncertainties of LAI Products

3.3.1. Spatial Consistency of LAI Relative Uncertainties

[25] The relative uncertainty maps differ among the LAI products (Figure 6). MODIS produces the lowest relative uncertainties and JRC-TIP produces the highest values. The largest discernible discrepancies occur in the boreal regions (60°N). The highest relative uncertainties are generally located in the ecological transition zones, such as the sparsely vegetated western parts of the Americas, Sahel, South Africa, central Asia, and Australia, as well as savanna areas. MODIS shows very low relative uncertainties in the eastern United States, Amazonia, central Africa, southeastern Asia, and the arctic regions. GEOV1 displays higher relative uncertainties than MODIS at lower latitudes but is lower than MODIS in the boreal regions. The relative uncertainties for GEOV1 are between 20% and 40% in the boreal regions during summer. The JRC-TIP relative uncertainties exhibit strong spatial variability in South America, Africa, and East Asia, especially in January. The relative uncertainties of JRC-TIP show more spatial variability than the other two products during summer.

3.3.2. Uncertainty-LAI Relationships

[26] Overall, the relative uncertainties for the three LAI products are in the following order: MODIS < GEOV1 < JRC-TIP (Table 3). The relative uncertainty for GEOV1 (26.6%) is more than twice that of MODIS (11.5%). For both MODIS and GEOV1, the relative uncertainties for broadleaf forests are lower than those for the needleleaf forests (Table 3). Figure 7 illustrates the general relationship between product uncertainties

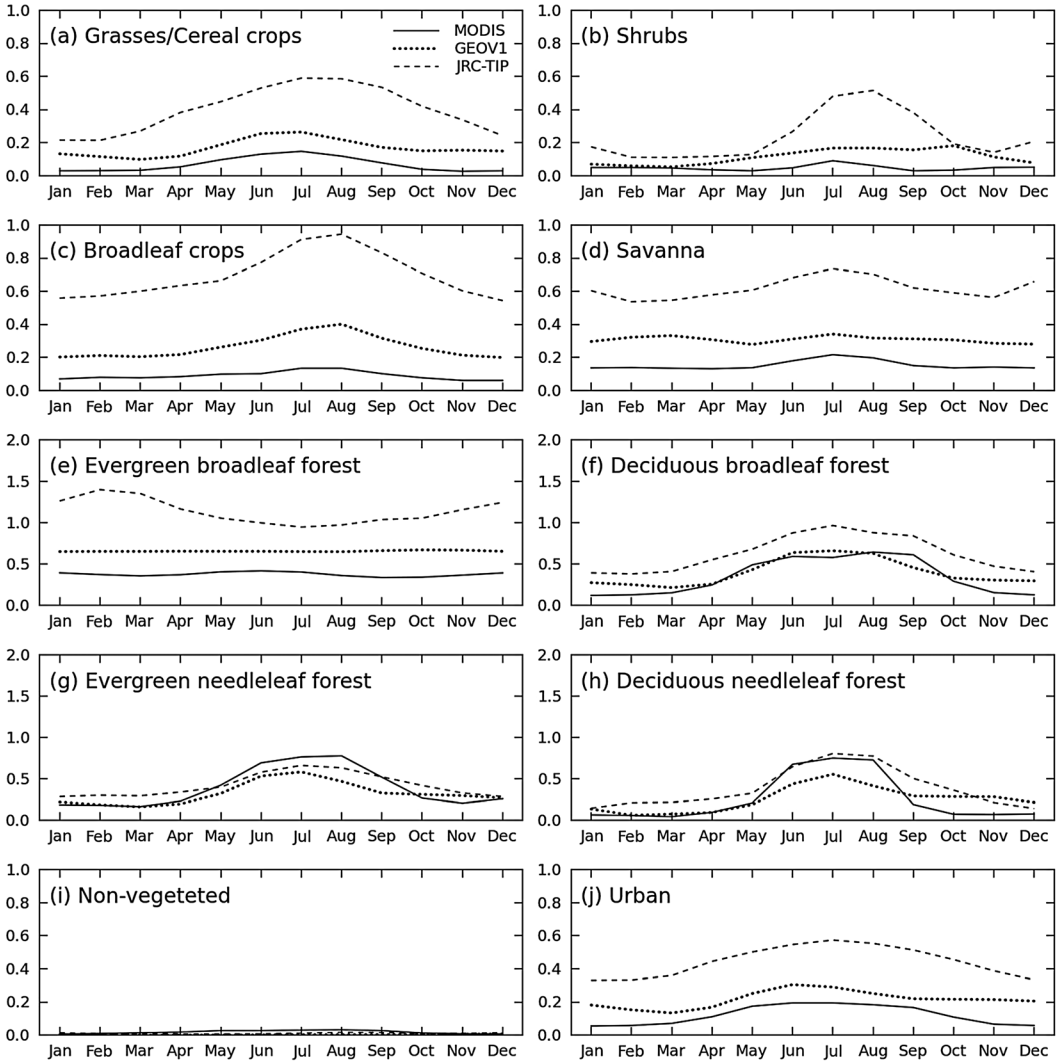

Figure 5. Climatologies of global LAI uncertainties for MODIS, GEOV1, and JRC-TIP from 2003 to 2010 (0.05°).

and LAI values. The uncertainties for MODIS and GEOV1 are about 10−14% of the LAI values (Figures 7a and 7b). For JRC-TIP, the overall uncertainty is about 52% of the LAI values, with an offset of 0.24 ($R^2 = 0.397$). The figure indicates that the uncertainties are largely modulated by LAI values, especially for GEOV1 ($R^2 = 0.843$). The strong linear relationship between GEOV1 uncertainty and LAI indicates that the relative uncertainties might be inherent to the properties of the product. In contrast, MODIS and JRC-TIP appear to have maximum product uncertainty fluctuations for intermediate LAI values at around 4.0 and 2.0, respectively.

[27] For each product, there are two LAI and uncertainty peaks, corresponding to the herbaceous and woody biome types, which can be clearly identified in the density scatter plots (Figure 7). For MODIS, the two peaks are located at LAI < 2 and between 5 and 6, respectively. For GEOV1, the locations of the two peaks are at LAI < 3 and between 4 and 5.5, respectively, and the uncertainty values are higher than those produced by MODIS. Figure 7b also shows that the GEOV1 LAI maximum is around 6.7, while the uncertainty peaks are around 1.0. The locations of the JRC-TIP peaks are at LAI < 1.3 and between 1.2 and 2.0, respectively, which illustrates the lower effective LAI values with relatively high uncertainties.

3.3.3. Temporal Variation in LAI Relative Uncertainties

[28] Figure 8 shows the climatologies of the relative uncertainties for MODIS, GEOV1, and JRC-TIP. In contrast to the LAI values and uncertainties, no consistent seasonal trends are observed for any particular biome type. For MODIS, small seasonal variations occur for DBF, ENF, and DNF, while the relative uncertainties are relatively stable for the other biome types. The MODIS relative uncertainties are less than 20% for all biomes, except for ENF (23.9%). The smallest relative uncertainty is observed for EBF (8.8%). For GEOV1, with the exception of EBF (15.9%), the relative uncertainties are all higher than 20%. In comparison, the relative uncertainties for MODIS are slightly lower than those of GEOV1 for all biome types, except for ENF. The largest deviations between the two products can be seen for nonforest biomes. The relative uncertainties for MODIS and GEOV1 show nearly no seasonal change for EBF. The overall relative uncertainty for

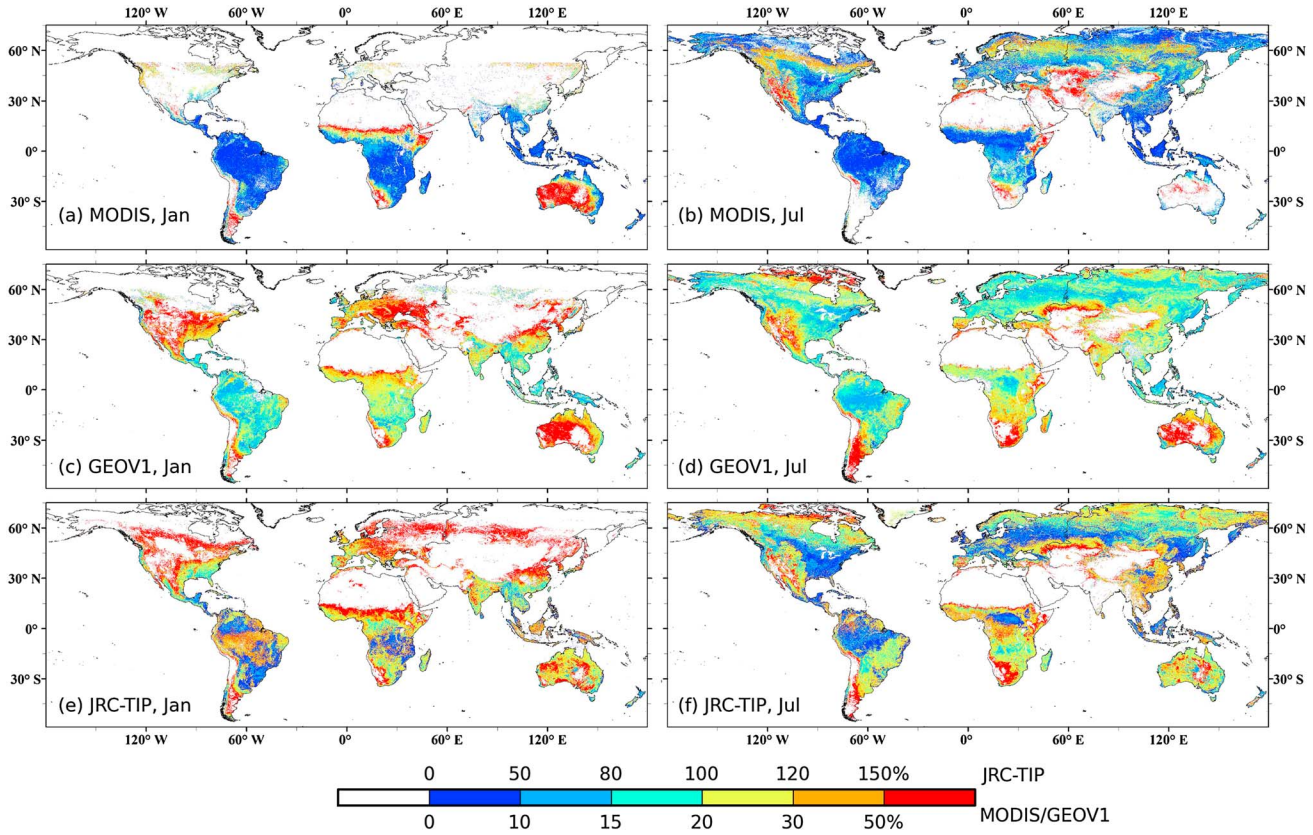

Figure 6. Maps of LAI relative uncertainties for MODIS, GEOV1, and JRC-TIP from 2003 to 2010 (0.05°) in January (left panels) and July (right panels), respectively. Note the different scale bar for JRC-TIP.

JRC-TIP reaches about 114.3% (Table 3). Because of the relatively lower values and higher uncertainties, the JRC-TIP profiles have extremely high relative uncertainties (> 100%) for most of the year, except during the summer when the relative uncertainties decrease to around 60% for DBF (Figure 8f).

3.4. Intercomparison of LAI Products in Africa

3.4.1. Spatial Characterization

[29] Figure 9 demonstrates the performances of the six LAI products in Africa in July 2010. The highest LAI values are observed in the tropical rainforest regions (> 5.0), but they vary substantially among the different products. For most of the other areas, all the products show moderately similar and low LAIs (< 2.0). However, MODIS contains some missing pixels in the rainforest regions, and the MODIS status map (not shown) reveals that these pixels correspond to poor retrievals caused by consistent cloud contamination in the data. GEOV1, GLOBMAP, and JRC-TIP also suffer from similar data gaps, especially along the Gulf of Guinea coast. In comparison, GLASS displays the most continuous LAI map, which is due to the integration of MODIS and CYCLOPES and the yearly neural network approach (section 2.3). GLOBMAP shows similar, but concentrated, high LAIs in the tropical areas but gives slightly lower values for other areas

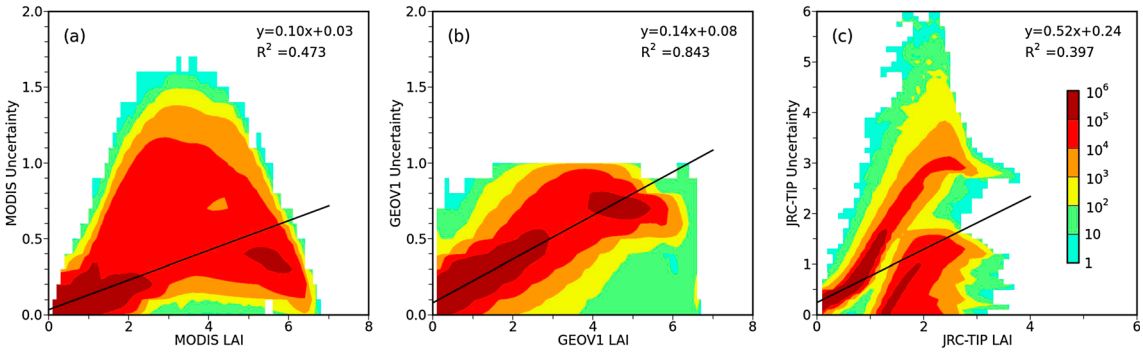

Figure 7. Density scatter plots between LAI and the associated uncertainties for (a) MODIS, (b) GEOV1, and (c) JRC-TIP.

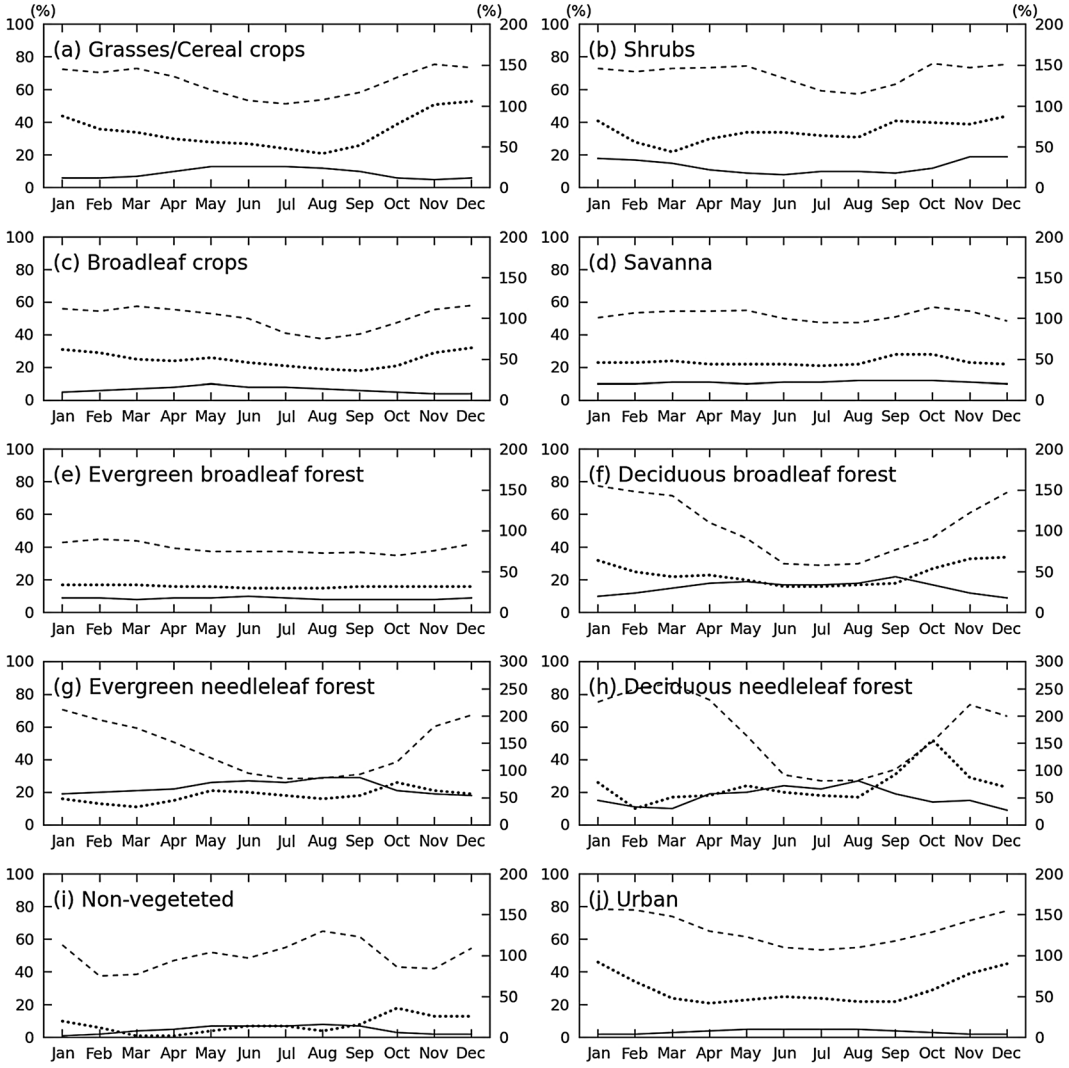

Figure 8. Climatologies of global LAI relative uncertainties (%) for MODIS (solid lines), GEOV1 (dotted lines), and JRC-TIP (dashed lines) from 2003 to 2010 (0.05°). See the left ordinates for MODIS and GEOV1, and the right ones for JRC-TIP. Same legend as in Figure 5.

in the continent. JRC-TIP is understandably lower (< 3.0) than all the other products, even for the tropical rainforest. Land-SAF is smaller in the equatorial areas but higher in the other regions compared to the other true LAI products. Land-SAF also reveals a uniquely smooth decreasing pattern from the tropical regions to higher latitudes because of its to more frequent observations and a monthly averaging of the daily values.

3.4.2. Land-SAF Uncertainties and Relative Uncertainties

[30] Figure 10 shows the Land-SAF uncertainties and relative uncertainties calculated in January and July between 2007 and 2010, respectively. The figure shows that the uncertainties for 10°N−18°S (> 0.2) are clearly higher than those of the other regions. The peak uncertainties migrate from the east Congo Basin in January (1.0–1.5) to the north Congo Basin in July (> 1.5), which corresponds to the seasonal migration of EBF in Africa [*Pfeifer et al*., 2012]. The relative uncertainties are relatively stable over the year and are lower between 5°N and 20°S (< 30%). The higher relative uncertainties (> 30%) are mainly distributed in the transitional zones between savanna, shrubs, and grasses.

3.4.3. Characterization of a Transect

[31] Figure 11 compares the LAIs, the uncertainties, and the relative uncertainties along the 25°E transect in July 2010. The curves were filtered using a 2.5° moving averaging method to show the general performances of the different products. From the furthest north to the furthest south, LAI values gradually increase from 15°N to 5°N and produce a maximum EBF value of around 5.0. After a sudden decrease to less than 2.0 along 4°S, the LAI values gradually decrease from woody savannas to open shrublands. The tropical areas (5°N−4°S) show rather marked differences for EBF, with LAI values varying from 3.4 (Land-SAF) to 5.2 (MODIS). This confirms the earlier observation of large deviations for EBF and will be discussed further in section 4.1. At subtropical latitudes (4°S−25°S, and 5°N−10°N), the landscape is dominated by savanna systems and the LAI values differ considerably between the different products. MODIS, GLASS, and Land-SAF produce similar values for woody savannas between 5°N and 8°N. However, GEOV1 produces higher, and GLOBMAP produces lower values (by about 1.0) than MODIS, GLASS, and Land-SAF.

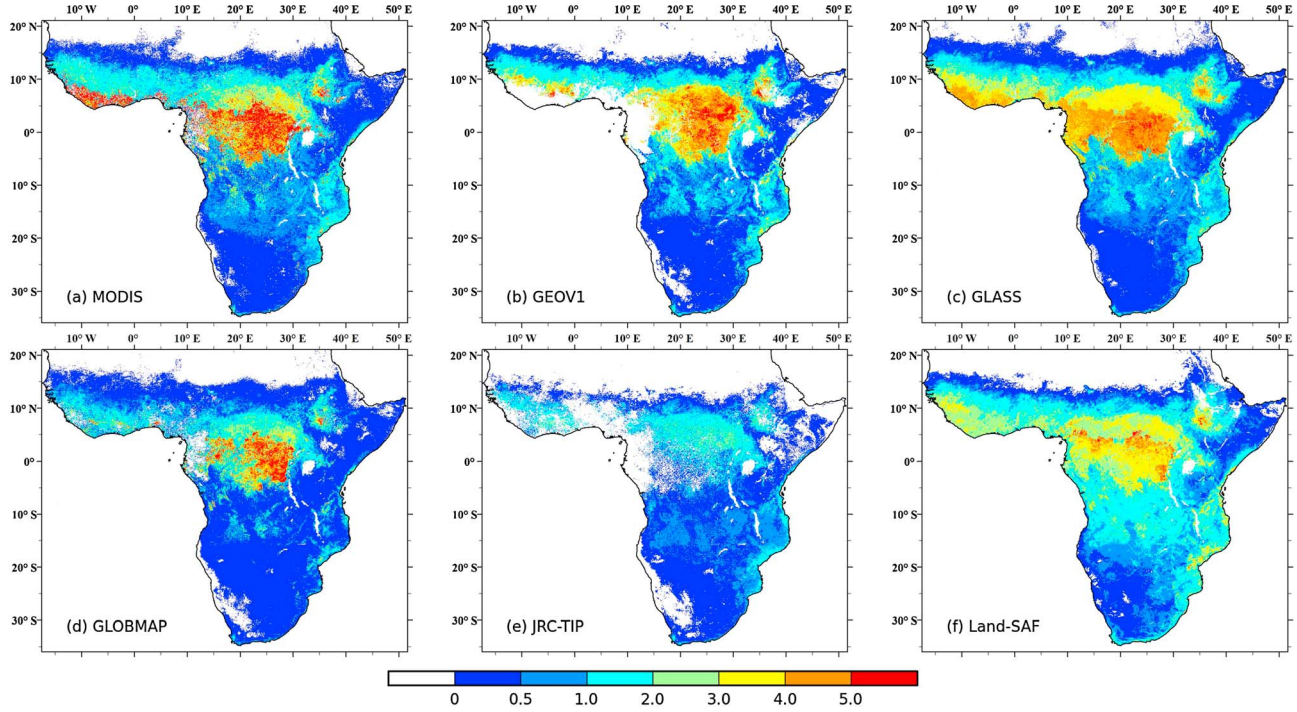

Figure 9. (a) MODIS, (b) GEOV1, (c) GLASS, (d) GLOBMAP, (e) JRC-TIP, and (f) Land-SAF LAI products in Africa in July 2010 (0.05°).

Substantial differences also exist between the two hemispheres for the savanna systems. Savannas and woody savannas in the northern hemisphere occur in a narrow latitudinal band (about 3°), but their LAI values are higher (~1.5) than those of their counterparts in the southern hemisphere. In contrast to the northern hemisphere, Land-SAF shows higher values than all the other products from 4°S southward. The peculiar performance of the savanna systems could be related to the unique vegetation structure of this biome type which is marked by a highly dynamic vegetation structure, varying across space and time and driven by precipitation seasonality [*Bucini and Hanan*, 2007; *Pfeifer et al*., 2012]. Some of these differences may also be related to the different product composition periods. For example, the daily Land-SAF product may be able to optimally capture the high frequent LAI changes caused by precipitation, whereas this sort of information may be missed by other products with a longer composition cycle.

[32] In a similar manner to LAI, the uncertainties are also higher for woody savannas and EBF (Figure 11b). The MODIS uncertainties are below 0.5 over the whole transect. The GEOV1 uncertainties are around 0.75 for both woody savannas and EBF. JRC-TIP and Land-SAF have similar profiles as the transect moves from 10°N to the south, reaching about 1.4 for woody savannas and EBF, but decreasing to < 0.5 for other latitudes. Land-SAF assigns a constant uncertainty value (0.3) to bare surfaces, such as the deserts at the two ends of Africa (from 10°N and from 15°S). The relative uncertainties produce bowl-shaped profiles with increasing values from lower to higher latitudes (Figure 11c). MODIS, GEOV1, and Land-SAF values are similar for savannas and EBF (10°N−19°S), which are slightly lower than the values for the other biome types at higher latitudes. The three products show relatively larger discrepancies for savannas and open shrublands from 19°S, which indicates the complex structures for these biome types. The relative uncertainties for JRC-TIP ($> 100\%$) are also lower for savannas and EBF than for grasslands and open shrublands.

3.5. Improvement Over Heritage Products

[33] The differences between the GEOV1 and GLOBMAP products and the heritage products are plotted in Figure 12. The improvement in GEOV1 over the earlier CYCLOPES is clear, both regarding accuracy and spatial and temporal consistency (not shown). CYCLOPES tends to underestimate MODIS, especially for higher LAI values, mainly due to the differences in LAI definitions between CYCLOPES (closer to effective LAI) and MODIS (true LAI) [*Fang et al*., 2012b]. In contrast, the global average GEOV1 value is slightly higher than that of MODIS (Table 3), and this is due to the new fusion algorithm (equation (1)). The MODIS-GEOV1 differences are much smaller than the previous MODIS-CYCLOPES differences [*Fang et al*., 2012b]. GEOV1 values have increased over the CYCLOPES values for all vegetated biomes, especially for the forest types (Figure 12a), indicating the effectiveness of the new fusion algorithm. The highest increase is found for EBF (~0.96). Geographically, GEOV1 matches better with MODIS in Amazon and boreal regions, whereas CYCLOPES usually underestimates MODIS in these regions [*Fang et al*., 2012b].

[34] The GEOV1 uncertainties are also smaller than those of CYCLOPES (Figure 12b). Substantial differences are found for broadleaf crops and savanna. For CYCLOPES, the typical uncertainties in summer are close to 0.80 and

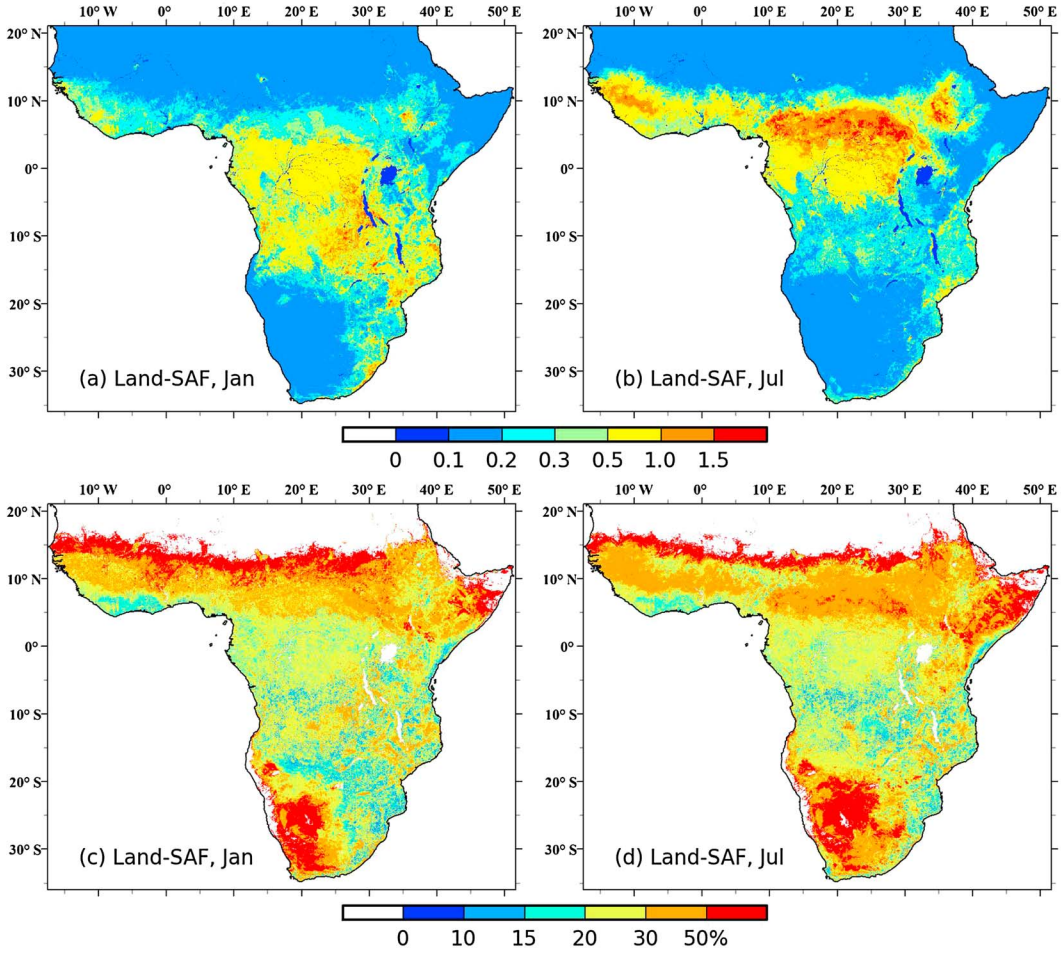

Figure 10. Land-SAF uncertainties (upper panels) and relative uncertainties (lower panels) in January and July, respectively (2007−2010, 0.05°).

0.70 for broadleaf crops and savanna, respectively [*Fang et al*., 2012c]. In comparison, the corresponding GEOV1 uncertainties are about 0.40 and 0.30, respectively. The reduction of the GEOV1 uncertainties (0.36 on average) are most significant for forest types, to a similar level with MODIS (Figure 5) which reaffirms the improvement of GEOV1 for these biome types. The relative uncertainty uniformly decreased by about 20−32% for all biomes (Figure 12c).

[35] Previous validation and intercomparison studies have shown that GLOBCARBON underestimates MODIS by about 1.0 for EBF due to algorithm differences and the different clumping processing methods [*ESA*, 2007; *Fang et al*., 2012b; *Garrigues et al*., 2008]. The present study reveals much improved spatial and temporal consistency between GLOBMAP and the other products for EBF. Overall, GLOBMAP has increased by about 1.5 over GLOBCARBON for EBF (Figure 12d). The improvement in consistency is mainly attributed to the enhanced MODIS reflectance data utilized in GLOBMAP [*He et al*., 2012; *Liu et al*., 2012].

3.6. Comparison With the GCOS Accuracy Requirement

[36] Figure 13 shows the percentage of pixels that falls within the GCOS quality thresholds for uncertainty (0.5) and relative uncertainty (20%). Based on a yearly average, 93.2% of MODIS pixels are within the GCOS quality requirement for uncertainty, followed by GEOV1 (85.8%) and JRC-TIP (74.5%). Seasonally, the number of pixels meeting the requirement is about 15% lower in summer than in winter for MODIS, GEOV1, and JRC-TIP, which reflects the higher LAI values and the associated retrieval uncertainties during the peak growing season. Land-SAF shows a minor seasonality, and about 82.0% of the data have met the quality requirement in continental Africa. This is comparable to that reported in the Land-SAF validation report, which states that the mean uncertainty is below 0.6 for 71% of the land surface [*García-Haro et al*., 2008]. With regard to different biome types, forested pixels have a slightly lower percentage of pixels than nonforest types that have met the quality requirement (Figure 13b). This is partly related to the generally higher LAI values and uncertainties for forests. EBF have the lowest percentage of pixels that have met the requirement for GEOV1 (17.1%), JRC-TIP (26.4%), and Land-SAF (17.8%), which indicates the difficulty of LAI retrieval for this biome type (section 4.1).

[37] With regard to the relative uncertainty threshold (20%), the number of good retrievals is ranked as follows: MODIS (78.5%) > GEOV1 (44.6%) > Land-SAF (13.3%) > JRC-TIP (5.7%). For GEOV1, the percentage of good retrievals shows small seasonal variations, ranging

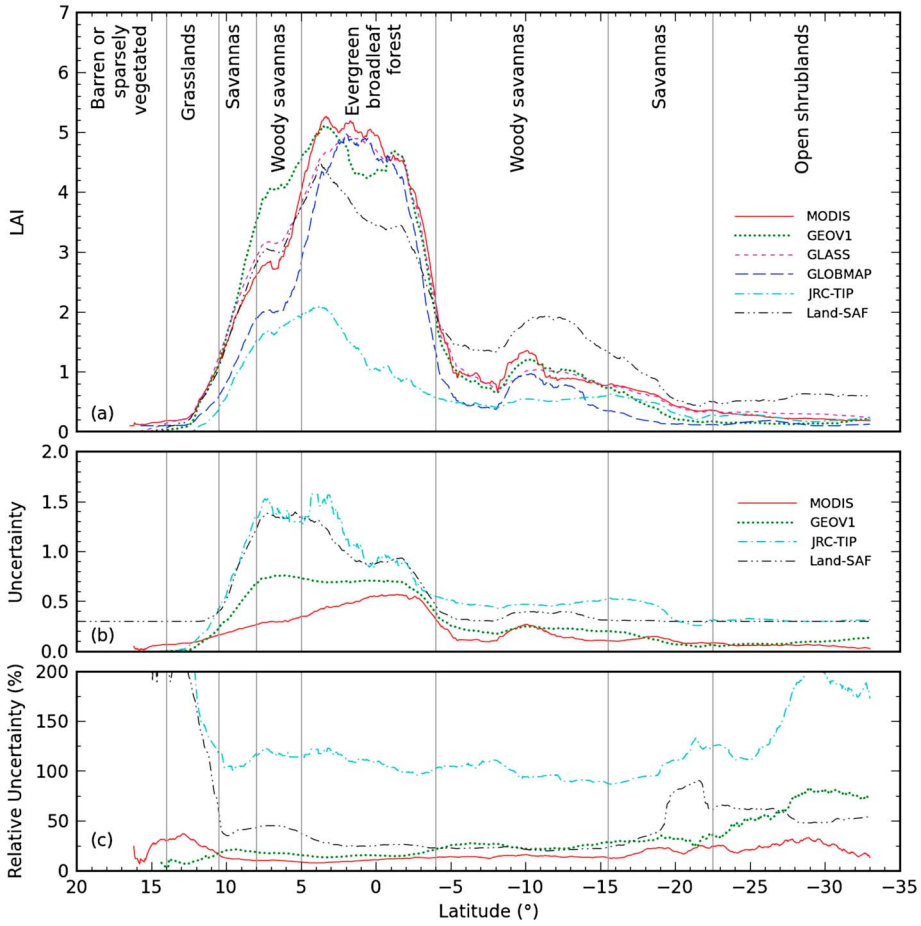

Figure 11. Transects of (a) LAI, (b) uncertainties, and (c) relative uncertainties over Africa (along 25°E) for July 2010. The land cover classes are based on the MODIS IGBP classification [*Friedl et al.*, 2010].

from 31.0% in October to 58.6% in August, whereas there are nearly no seasonal changes for the other three products (Figure 13c). Pixels with good retrievals are distributed over various biome types (Figure 13d). Unlike the absolute uncertainties (Figure 13b), there is no clear dominant contributing biome type for the relative uncertainties (Figure 13d).

[38] In this study, the theoretical uncertainties are derived by each product separately, using different approaches, tools, and resolutions. In order to consolidate the differences in product uncertainties, a triple collocation error model (TCEM) has been developed to calculate theoretical uncertainties for the MODIS, CYCLOPES, and GLOBCARBON LAI

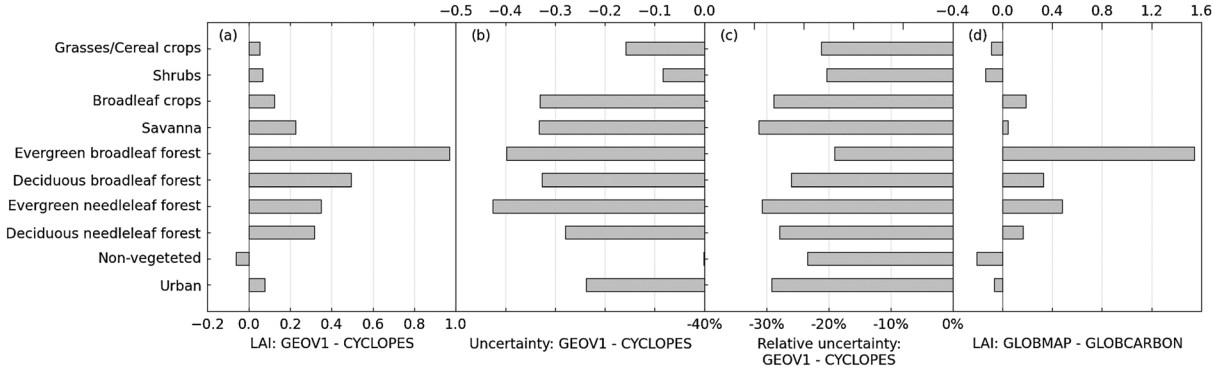

Figure 12. Bar plots showing the differences between GEOV1 and GLOBMAP with CYCLOPES and GLOBMAP, respectively. (a) Mean LAI differences between GEOV1 and CYCLOPES, (b) uncertainty differences between GEOV1 and CYCLOPES, (c) relative uncertainties differences between GEOV1 and CYCLOPES, and (d) mean LAI differences between GLOBMAP and GLOBCARBON.

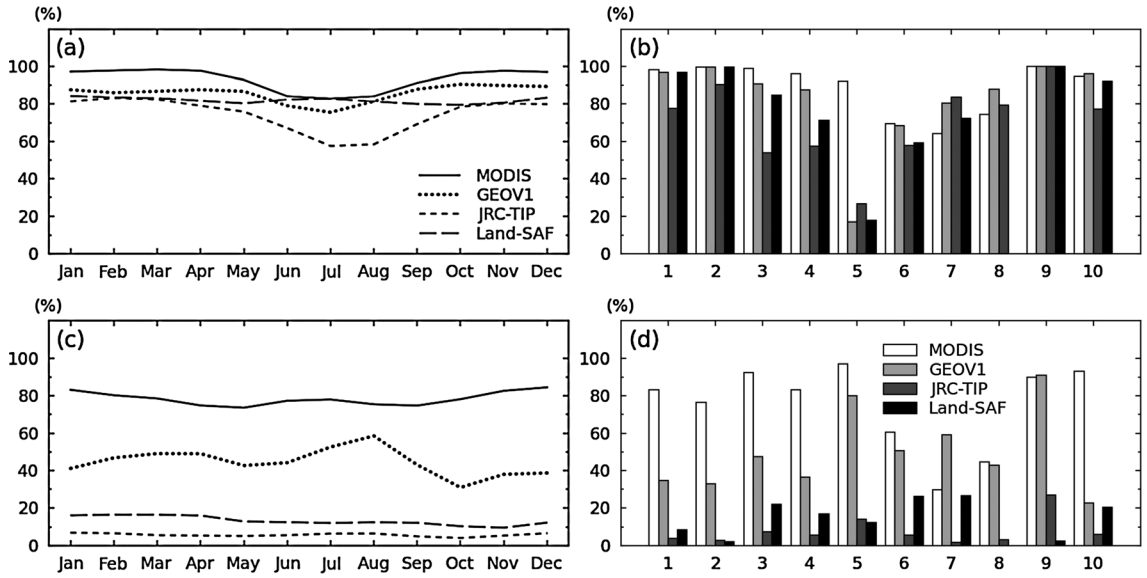

Figure 13. Percentages of MODIS, GEOV1, JRC-TIP, and Land-SAF pixels that meet the quality requirements for (a and b) uncertainties and (c and d) relative uncertainties, respectively. (b and d) The statistics for different biome types. Land-SAF for Africa only. Percentages calculated as the ratio of the number of pixels that meet the threshold to the total number of valid retrievals. Biome types 1−10 correspond to Figures 2a–2j.

products [*Fang et al*., 2012c]. The results from this study (Table 3) show that the average uncertainties (< 0.50) and the relative uncertainties (< 40%) are comparable to those estimated by TCEM, which shows the validity of exploring theoretical uncertainties using both product QQIs and the TCEM approach. The TCEM study [*Fang et al*., 2012c] indicates that less than 39.5% of MODIS and nearly half of CYCLOPES retrievals (49.1%) have met the quality requirement for absolute uncertainty (0.5). With regard to the relative uncertainties, the percentages of good retrievals are only 19.2% and 37.7% for MODIS and CYCLOPES, respectively. Results from the present study indicate that the relative uncertainties associated with the products clearly have a significantly higher percentage of good retrievals compared to those obtained using the independent TCEM approach. These differences reflect the different approaches in deriving the theoretical uncertainties and should be considered in evaluating the product uncertainties.

4. Discussion

4.1. Characteristics of the Global LAI Products

[39] By definition, all the LAI products, except for JRC-TIP, represent the true LAI. For GEOV1, the essence of the fusion process (equation (1)) is to reduce the contribution of MODIS for low LAI values, while enhancing its contribution for larger values. GLASS shows the greatest similarity to MODIS and GEOV1 (Figure 3) because it fuses the best MODIS and CYCLOPES estimates, biome by biome, and uses the MODIS reflectance as an input. GLOBMAP shows a generally good agreement with MODIS but with slightly lower values for broadleaf crops (by about 0.2−0.5), savanna (~0.5), and EBF (~0.5). The GLOBMAP underestimation of broadleaf crops and savanna can be partly explained by the mismatch between the land cover types adopted by different retrieval algorithms. The MODIS LAI algorithm separates grasses/cereal crops and broadleaf crops, while GLOBMAP combines them into one type (crops, grasses, and others). Likewise, GLOBMAP combines shrubs and savanna into shrubs in the LAI algorithm. JRC-TIP is understandably lower and is about one third of the other true LAI values. The JRC-TIP product is likely bounded by the upper limit (3.0 or slightly higher) for the effective LAI values [*Pinty et al*., 2011a]. Land-SAF LAI values are relatively smooth because SEVIRI high-frequency sampling largely alleviates the cloudiness problem experienced by optical-infrared sensors and small fragmented clouds are usually averaged over time.

[40] This study demonstrates that even with the same MODIS input reflectance, GLASS and GLOBMAP result in larger discrepancies (~0.5) for broadleaf crops and savanna than other biome types. The differences are due to the different LAI retrieval methods, clumping effect processing, and incorporation of a priori information. GLASS algorithms treat the yearly reflectance data as a whole, whereas GLOBMAP processes every 8 day period separately. GLASS algorithms use the biome-specific clumping information as a priori model input, whereas GLOBMAP needs the pixel-based clumping index to convert the effective LAI to the true LAI.

[41] Retrieving accurate LAI values from very dense canopies remains a challenging task [*Aragão et al*., 2005; *Shabanov et al*., 2005]. The disagreement between the LAI products (< 1.0) is notable for EBF. This confirms earlier findings that large discrepancies exist for EBF due to reflectance saturation and cloud-aerosol contamination [*Fang et al.*, 2012b; *Garrigues et al*., 2008]. Severe underestimation has been reported for CYCLOPES, which gives consistently lower LAI estimates than MODIS [*Fang et al.*, 2012b; *Weiss et al*., 2007]. Evidently, GEOV1 has improved the correspondence, as compared to CYCLOPES, with MODIS for this biome type and has also improved the results for low LAI periods in tropical evergreen

vegetation caused by persistent cloud cover [*Myneni et al*., 2007]. GLOBMAP underestimation of EBF has also been reported previously [*Liu et al*., 2012]. The underestimation by Land-SAF, with regard to other true LAI products, for EBF in Africa (Figure 11a) highlights the algorithm differences and the complexity of this biome type. New cloud and aerosol detection techniques based on time series and spatial analyses may help to reduce these uncertainties and improve LAI estimation of EBF [*Hilker et al*., 2012].

[42] ENF and DNF show similar seasonal courses but different amplitudes in winter (Figure 2). For ENF, the average true LAI values rise from about 0.93 in January to 3.49 in July. The seasonal variation in ENF is mainly attributed to changes in the understory [*Heiskanen et al*., 2012; *Manninen et al*., 2012]. Several studies have indicated that the winter LAI for ENF has been unrealistically underestimated by current LAI products [*Fang et al*., 2012c; *Garrigues et al*., 2008; *Tian et al*., 2004]. Accurate estimation of LAI in needleleaf forests in winter is challenging because of poor illumination conditions, low solar zenith angle (SZA), snow and cloud contamination, and the signal from the understory [*Pisek et al*., 2010; *Weiss et al*., 2007]. These issues clearly have negative impacts on LAI data quality and their applications. How to improve the LAI estimation in winter should be a crucial research topic in the future.

4.2. Interpretation of LAI Uncertainties

[43] The product uncertainties and the spatial and temporal variability are largely correlated with the LAI values. The present study has indicated the general spatial and temporal consistency of the product uncertainties between MODIS and GEOV1 (Figures 4 and 5). However, no strong relationship ($R^2 < 0.39$) was noticed globally between the various uncertainties (not shown), which reveals the different schemes used in the uncertainty computation. For the relative uncertainties, there are no clear seasonal and latitudinal trends, indicating that the relative uncertainty might be an inherent property of the products. The relatively high errors obtained in the ecological transition zones (Figure 6) are attributed to the mixed land cover types [*Hu et al*., 2003], which make LAI retrieval difficult. The different performances between MODIS and GEOV1 reflect the impact of the input reflectances, the solar zenith angles, the retrieval algorithms, and the treatment of biome types [*Myneni et al*., 2002; *Weiss et al*., 2007]. It should be noted that no a priori biome classification information has been used in the GEOV1 algorithm. JRC-TIP tends to have large relative uncertainties ($> 100\%$) for DBF, ENF, and DNF in winter and spring (October to May), which is probably due to the understory exposure when the satellite observes mixed signals from the understory and the background [*Pisek et al*., 2010].

[44] The present study of theoretical uncertainty is complementary to other validation studies which have provided LAI physical uncertainties. It should be noted that the theoretical uncertainties obtained in the present study (Table 3) are all smaller (by half) than the physical uncertainties reported in recent validation studies, which generally vary from 1.06 to 1.37 for MODIS, from 0.50 to 1.24 for CYCLOPES [*Fang and Liang*, 2005; *Fang et al*., 2012a; *Garrigues et al*., 2008; *Verger et al*., 2009; *Weiss et al*., 2007], and are around 1.15 for GLOBCARBON [*Garrigues et al*., 2008]. The very low theoretical uncertainty values should be interpreted in relation to the differences in theoretical and physical uncertainties.

[45] The relative uncertainties for MODIS and GEOV1 (Table 3) are also smaller than the relative physical uncertainties obtained in recent studies, which can range from 30 to 80% [*Gonsamo*, 2010; *Pinty et al*., 2007; *Pisek and Chen*, 2007; *Verger et al*., 2009]. The relative uncertainty for Land-SAF appears to be higher than that of the specified target accuracy (25−30%) [*García-Haro et al*., 2008]. The large relative uncertainty for JRC-TIP attests to the different characteristics of the LAI retrieval algorithms and the product QQIs, which suggests a need for further investigation into the effective LAI product.

4.3. Limitations and Future Studies

[46] Any intercomparison study is hampered by several factors: (1) differences in concepts and definitions, (2) algorithm differences, (3) discrepancies in temporal and spatial referencing, and (4) the mismatch between land cover types. In this study, the uncertainty information provided by each product is derived using different approaches, tools, and input products. Variances in the input data and the strong nonlinearity of the LAI retrieval algorithm may also translate into uncertainty values that may exceed those specified a priori in the algorithm. Differences in the pixel sizes and the temporal compositing period are to be expected for the LAI products. The impact of biome misclassification on LAI estimation has been investigated in a number of studies [*Fang et al*., 2013; *Gonsamo and Chen*, 2011; *Myneni et al*., 2002]. Global averaging over all pixels of a particular biome type may also mask the underlying variability in LAI amongst those pixels. Given these inherent issues, it is hard to conclude which is the best single quality indicator for representing LAI uncertainty.

[47] A hierarchical four-stage validation approach has been adopted by the Committee on Earth Observation Satellites (CEOS), following the recommendations of the Land Product Validation (LPV) group [http://landval.gsfc.nasa.gov/, *Morisette et al*., 2006]. Intercomparison of independent products, as demonstrated in the present study, corresponds to the third validation scheme proposed by the LPV to develop product uncertainty information. The MODIS LAI product has achieved Stage 2 validation [*Nightingale et al*., 2009]. Stage 3 validation involves assessing product accuracy via independent measurements that represent global conditions [http://landval.gsfc.nasa.gov/]. With this and other similar studies [*Fang et al*., 2012a, 2012b, 2012c; *Garrigues et al*., 2008; *Weiss et al*., 2007], Stage 3 validation for global LAI products can be achieved.

[48] Further work should focus on the development of improved methods for LAI estimation. Even with the availability of product quality indicators, further validation efforts should be made in order to obtain absolute values of product reliability and accuracy. In-depth Stage 3 validation should involve more comprehensive field data collection for under-represented biome types and areas. The present findings for Land-SAF in Africa will be updated when new products with global coverage are available. With the advent of several operational LAI products, there is a trend to generate the best LAI estimates from existing products (e.g., GEOV1 and GLASS). However, how errors accumulate during the fusion

process needs to be investigated. This study also reveals the importance for data users to refer to the product QQIs. Meanwhile, it is important for data producers to provide the quality indicators. Results from this study should therefore be further interpreted with new knowledge about the product uncertainties.

5. Conclusions

[49] In this study, five global LAI products—MODIS, GEOV1, GLASS, GLOBMAP, and JRC-TIP—were assessed by examining their climatologies and uncertainty information for different biome types. All the LAI products generally agree with each other in representing the LAI temporal variation, while discrepancies are observed with regard to LAI levels, mainly due to differences between definitions, retrieval methodologies, and input data. The products agree remarkably well for grasses, crops, shrubs, and savanna, with typical absolute differences below 0.5. For forests, the deviations among the products are less than 1.0, and MODIS, GEOV1, GLASS, and GLOBMAP strongly correlate with each other ($R^2 > 0.74$). The effective JRC-TIP LAI values are about half the values produced by the other products. Conversion equations between different products will help alleviate the differences in definitions and residual errors caused by different algorithms and input data. Continental assessment of LAI products shows that Land-SAF is consistent with the other products in Africa, although small discrepancies (< 1.0) do exist for woody savannas and evergreen broadleaf forest.

[50] This study is the first to explore the product quantitative quality indicators (QQIs) embedded in the LAI products. The theoretical uncertainties are related to the LAI values, and both exhibit consistent seasonal variability. Generally, the forested areas display higher uncertainties than the agricultural areas. The MODIS uncertainty is less than 0.2 for nonforest biomes and less than 0.5 for forest types. For GEOV1, the uncertainty is < 0.3 for all biome types, except for evergreen broadleaf forest (0.50). The overall uncertainty is highest (0.43) for JRC-TIP but moderate for Land-SAF (0.36). The derived relative uncertainties are variable across regions and appear to increase in ecological transition zones. However, no clear seasonal trends are observed for the relative uncertainties, indicating that the relative uncertainty might be an inherent property of the products. Averaged globally, the relative uncertainties are in the following order: MODIS (11.5%) < GEOV1 (26.6%) < Land-SAF (37.8%) < JRC-TIP (114.3%). MODIS and GEOV1 generally show a similar range of relative uncertainties in summer. For JRC-TIP, the climatologies of the relative uncertainties show rather large temporal variations, marked by higher deviations during winter and spring. In contrast to the usually prescribed LAI uncertainties in land surface modeling studies, the product QQIs allow a more convenient specification of LAI uncertainties and temporal variability at the grid level.

[51] Theoretically, the absolute uncertainty indicators demonstrate that more than 75% of MODIS, GEOV1, JRC-TIP, and Land-SAF pixels have met the absolute uncertainty requirements ($\pm$ 0.5) set by GCOS. Among the biome types, evergreen broadleaf forest is the dominant contributor to the number of pixels that fails to meet the quality threshold. In terms of the relative uncertainty, more than 78.5% of MODIS and 44.6% of GEOV1 pixels have met the minimum accuracy requirement (20%). However, $< 15\%$ of the Land-SAF and JRC-TIP pixels have met the quality requirement for relative uncertainties. It should be noted that the reported theoretical uncertainties are all smaller than the physical uncertainties revealed by recent independent validation studies [*Fang et al.*, 2012a]. The theoretical uncertainties explored in this study point the way for further validation studies of physical uncertainties.

[52] This study provides an operational guideline for further studies to understand and improve the accuracy of global LAI products. For example, by taking advantage of existing high-quality products, GEOV1 and GLASS have improved over the earlier CYCLOPES and GLOBCARBON, in terms of spatial and temporal consistency and similarity to MODIS. Future studies should focus on areas (e.g., ecological transition zones) and periods (e.g., winter time) where there are higher uncertainties. With the advances in instrument and retrieval algorithms, further cross-validation studies should be performed in the future, which should lead to the rational assessment of product qualities. As only theoretical uncertainties were explored in this study, product physical uncertainties warrant further investigation. The current method can be adapted for the cross-validation of other essential climate variables, such as the fraction of photosynthetically active radiation absorbed by vegetation (FPAR) and albedo.

[53] **Acknowledgments.** This study was partially supported by the Hundred Talent Program of the Chinese Academy of Sciences and the National Natural Science Foundation of China (41171333) (H.F.). The GLASS project was supported by the State Program for High-Tech Research and Development (863 program) (2009AA122100) and National Basic Research Program of China (973 Program) (2007CB714407). The GLOBMAP project was funded by the National Basic Research Program of China (2010CB950701). We thank all the web teams who facilitated the distribution of global LAI products: WIST (http://wist.echo.nasa.gov, accessed on 1 March 2012), the Geoland2 project (http://www.gmes-geoland.info), the BNU data center (http://www.bnu-datacenter.com/ or http://glass-product.bnu.edu.cn/), the GLOBMAP (http://www.globalmapping.org/globalLAI/), and the Land-SAF project (http://landsaf.meteo.pt/).

References

Abuelgasim, A. A., R. A. Fernandes, and S. G. Leblanc (2006), Evaluation of national and global LAI products derived from optical remote sensing instruments over Canada, *IEEE Trans. Geosci. Remote Sens.*, *44*(7), 1872–1884, doi:10.1109/TGRS.2006.874794.

Aragão, L. E. O. C., Y. E. Shimabukuro, F. D. B. Espirito Santo, and M. Williams (2005), Spatial validation of collection 4 MODIS LAI product in eastern Amazonia, *IEEE Trans. Geosci. Remote Sens.*, *43*(11), 2526–2534, doi:10.1109/TGRS.2005.856632.

Barbu, A. L., J. C. Calvet, J. F. Mahfouf, C. Albergel, and S. Lafont (2011), Assimilation of Soil Wetness Index and Leaf Area Index into the ISBA-A-gs land surface model: Grassland case study, *Biogeosciences*, *8*(7), 1971–1986, doi:10.5194/bg-8-1971-2011.

Baret, F., J. Morissette, R. Fernandes, J. L. Champeaux, R. Myneni, J. Chen, S. Plummer, M. Weiss, C. Bacour, and G. Derive (2006), Evaluation of the representativeness of networks of sites for the global validation and intercomparison of land biophysical products: Proposition of the CEOS-BELMANIP, *IEEE Trans. Geosci. Remote Sens.*, *44*(7), 1794–1803, doi:10.1109/TGRS.2006.876030.

Baret, F., et al. (2007), LAI, fPAR, and fCover CYCLOPES global products derived from VEGETATION Part 1: Principles of the algorithm, *Remote Sens. Environ.*, *110*(3), 275–286, doi:10.1016/j.rse.2007.02.018.

Baret, F., M. Weiss, R. Lacaze, F. Camacho, H. Makhmara, P. Pacholcyzk, and B. Smets (2013), GEOV1: LAI, FAPAR essential climate variables and FCOVER global time series capitalizing over existing products.

Part1: Principles of development and production, *Remote Sensing of Environment*, doi:10.1016/j.rse.2012.12.027, in press.

Bucini, G., and N. P. Hanan (2007), A continental-scale analysis of tree cover in African savannas, *Glob. Ecol. Biogeogr.*, *16*, 593–605, doi:10.1111/j.1466-8238.2007.00325.x.

Camacho, F., F. Baret, J. Cernicharo, R. Lacaze, and M. Weiss (2010), Quality assessment of the first version of Geoland-2 biophysical variables produced at global scale, paper presented at the Third International Symposium on Recent Advances in Quantitative Remote Sensing, Torrent, Spain, September 27–October 1, 2010, pp. 660–665.

Chen, J. M., and S. G. Leblanc (1997), A four-scale bidirectional reflectance model based on canopy architecture, *IEEE Trans. Geosci. Remote Sens.*, *35*, 1316–1337, doi:10.1109/36.628798.

Chen, J. M., C. H. Menges, and S. G. Leblanc (2005), Global mapping of foliage clumping index using multi-angular satellite data, *Remote Sens. Environ.*, *97*(4), 447–457, doi:10.1016/j.rse.2005.05.003.

De Kauwe, M. G., M. I. Disney, T. Quaife, P. Lewis, and M. Williams (2011), An assessment of the MODIS collection 5 leaf area index product for a region of mixed coniferous forest, *Remote Sens. Environ.*, *115*(2), 767–780, doi:10.1016/j.rse.2010.11.004.

Deng, F., J. M. Chen, S. Plummer, M. Chen, and J. Pisek (2006), Algorithm for global leaf area index retrieval using satellite imagery, *IEEE Trans. Geosci. Remote Sens.*, *44*(8), 2219–2229, doi:10.1109/TGRS.2006.872100.

Drusch, M., F. Gascon, and M. Berger (2010), GMES Sentinel-2 Mission Requirements Document, Reference Number: EOP-SM/1163/MR-dr, pp. 38, http://esamultimedia.esa.int/docs/GMES/Sentinel-2_MRD.pdf.

ESA (2007), GLOBCARBON DPQRv4.2 Demonstration Products and Qualification Report, pp. 69, http://due.esrin.esa.int/prjs/prjs43.php.

Fang, H., and S. Liang (2005), A hybrid inversion method for mapping leaf area index from MODIS data: Experiments and application to broadleaf and needleleaf canopies, *Remote Sens. Environ.*, *94*(3), 405–424, doi:10.1016/j.rse.2004.11.001.

Fang, H., S. Wei, and S. Liang (2012a), Validation of MODIS and CYCLOPES LAI products using global field measurement data, *Remote Sens. Environ.*, *119*, 43–54, doi:10.1016/j.rse.2011.12.006.

Fang, H., S. Wei, and C. Jiang (2012b), Intercomparison and uncertainty analysis of global MODIS, CYCLOPES, and GLOBCARBON LAI products, paper presented at the 2012 IEEE International Geoscience and Remote Sensing Symposium (IGARSS), Munich, Germany, July 22–27, 2012, pp. 5959–5962.

Fang, H., W. Li, and R. B. Myneni (2013), The impact of potential land cover misclassification on MODIS leaf area index (LAI) estimation: A statistical perspective, *Remote Sens.*, *5*(2), 830–844, doi:10.3390/rs5020830.

Fang, H., S. Wei, C. Jiang, and K. Scipal (2012c), Theoretical uncertainty analysis of global MODIS, CYCLOPES and GLOBCARBON LAI products using a triple collocation method, *Remote Sens. Environ.*, *124*, 610–621, doi:10.1016/j.rse.2012.06.013.

Friedl, M. A., D. Sulla-Menashe, B. Tan, A. Schneider, N. Ramankutty, A. Sibley, and X. Huang (2010), MODIS Collection 5 global land cover: Algorithm refinements and characterization of new datasets, *Remote Sens. Environ.*, *114*(1), 168–182, doi:10.1016/j.rse.2009.08.016.

García-Haro, F. J., F. Camacho-de Coca, and J. Meliá (2008), Product User Manual (PUM) of Land Surface Analysis Vegetation Parameters (FVC, LAI, FAPAR), Reference Number: SAF/LAND/UV/VR_VEGA/2.1, pp. 53, http://landsaf.meteo.pt/.

Garrigues, S., et al. (2008), Validation and intercomparison of global Leaf Area Index products derived from remote sensing data, *J. Geophys. Res.*, *113*, G02028, doi:10.1029/2007JG000635.

GCOS (2007), GCOS Observation Requirements in WMO/CEOS Database (incl ECVs), pp. 4, http://www.wmo.int/pages/prog/gcos/documents/GCOS_WCRP_ObservationRqmts_July2007_ECV.pdf.

GCOS (2011), Systematic Observation Requirements for Satellite-Based Products for Climate, 2011 Update, Supplemental Details to the Satellite-Based Component of the Implementation Plan for the Global Observing System for Climate in Support of the UNFCCC (2010 Update), Reference Number GCOS-154, pp. 138, http://www.wmo.int/pages/prog/gcos/Publications/gcos-154.pdf.

Gobron, N., and M. M. Verstraete (2009), Assessment of the Status of the Development of the Standards for the Terrestrial Essential Climate Variables: Leaf Area Index (LAI), Version 10, pp. 12, Global Terrestrial Observing System, Rome, http://www.fao.org/gtos/doc/ECVs/T11/T11.pdf.

Gonsamo, A. (2010), Leaf area index retrieval using gap fractions obtained from high resolution satellite data: Comparisons of approaches, scales and atmospheric effects, *Int. J. Appl. Earth Obs. Geoinf.*, *12*(4), 233–248, doi:10.1016/j.jag.2010.03.002.

Gonsamo, A., and J. M. Chen (2011), Evaluation of the GLC2000 and NALC2005 land cover products for LAI retrieval over Canada, *Can. J. Remote Sens.*, *37*(3), 302–313, doi:10.5589/m11-039.

He, L., J. M. Chen, J. Pisek, C. B. Schaaf, and A. H. Strahler (2012), Global clumping index map derived from the MODIS BRDF product, *Remote Sens. Environ.*, *119*, 118–130, doi:10.1016/j.rse.2011.12.00.

Heiskanen, J., M. Rautiainen, P. Stenberg, M. Mõttus, V.-H. Vesanto, L. Korhonen, and T. Majasalmi (2012), Seasonal variation in MODIS LAI for a boreal forest area in Finland, *Remote Sens. Environ.*, *126*, 104–115, doi:10.1016/j.rse.2012.08.001.

Hilker, T., A. I. Lyapustin, C. J. Tucker, P. J. Sellers, F. G. Hall, and Y. Wang (2012), Remote sensing of tropical ecosystems: Atmospheric correction and cloud masking matter, *Remote Sens. Environ.*, *127*, 370–384, doi:10.1016/j.rse.2012.08.035.

Hu, J., J. V. Martonchik, D. J. Diner, Y. Knyazikhin, R. B. Myneni, B. Tan, N. Shabanov, and K. A. Crean (2003), Performance of the MISR LAI and FPAR algorithm: A case study in Africa, *Remote Sens. Environ.*, *88*(3), 324–340, doi:10.1016/j.rse.2003.05.002.

Huang, D., Y. Knyazikhin, W. Wang, D. W. Deering, P. Stenberg, N. Shabanov, B. Tan, and R. B. Myneni (2008), Stochastic transport theory for investigating the three-dimensional canopy structure from space measurements, *Remote Sens. Environ.*, *112*(1), 35–50, doi:10.1016/j.rse.2006.05.026.

Jarlan, L., G. Balsamo, S. Lafont, A. Beljaars, J. C. Calvet, and E. Mougin (2008), Analysis of leaf area index in the ECMWF land surface model and impact on latent heat and carbon fluxes: Application to West Africa, *J. Geophys. Res.*, *113*, D24117, doi:10.1029/2007jd009370.

Knyazikhin, Y., J. V. Martonchik, R. B. Myneni, D. J. Dine, and S. W. Running (1998a), Synergistic algorithm for estimating vegetation canopy leaf area index and fraction of absorbed photosynthetically active radiation from MODIS and MISR data, *J. Geophys. Res.*, *103*, 32,257–232,276.

Knyazikhin, Y., J. V. Martonchik, D. J. Diner, R. B. Myneni, M. Verstraete, B. Pinty, and N. Gobron (1998b), Estimation of vegetation canopy leaf area index and fraction of absorbed photosynthetically active radiation from MISR data, *J. Geophys. Res.*, *103*, 32,239–232,256.

Knyazikhin, Y., et al. (1999), MODIS Leaf Area Index (LAI) and Fraction of Photosynthetically Active Radiation Absorbed by Vegetation (FPAR) Product (MOD15) Algorithm Theoretical Basis Document, pp. 126, http://modis.gsfc.nasa.gov/data/atbd/land_atbd.php.

Kobayashi, H., R. Suzuki, and S. Kobayashi (2007), Reflectance seasonality and its relation to the canopy leaf area index in an eastern Siberian larch forest: Multi-satellite data and radiative transfer analyses, *Remote Sens. Environ.*, *106*(2), 238–252, doi:10.1016/j.rse.2006.08.011.

Lafont, S., Y. Zhao, J. C. Calvet, P. Peylin, P. Ciais, F. Maignan, and M. Weiss (2012), Modelling LAI, surface water and carbon fluxes at high-resolution over France: Comparison of ISBA-A-gs and ORCHIDEE, *Biogeosciences*, *9*(1), 439–456, doi:10.5194/bg-9-439-2012.

Liu, Y., R. Liu, and J. M. Chen (2012), Retrospective retrieval of long-term consistent global leaf area index (1981–2011) from combined AVHRR and MODIS data, *J. Geophys. Res.—Biogeosci.*, *117*, G04003, doi:10.1029/2012JG002084.

Manninen, T., L. Korhonen, P. Voipio, P. Lahtinen, and P. Stenberg (2012), Airborne estimation of boreal forest LAI in winter conditions: A test using summer and winter ground truth, *IEEE Trans. Geosci. Remote Sens.*, *50*(1), 68–74, doi:10.1109/TGRS.2011.2173939.

Morisette, J. T., et al. (2006), Validation of global moderate-resolution LAI products: a framework proposed within the CEOS land product validation subgroup, *IEEE Trans. Geosci. Remote Sens.*, *44*(7), 1804–1817, doi:10.1109/TGRS.2006.872529.

Myneni, R., et al. (2007), Large seasonal changes in leaf area of amazon rainforests, *Proc. Natl. Acad. Sci.*, *104*(12), 4820–4823, doi:10.1073/pnas.0611338104.

Myneni, R. B., et al. (2002), Global products of vegetation leaf area and fraction absorbed PAR from year one of MODIS data, *Remote Sens. Environ.*, *83*(1–2), 214–231, doi:10.1016/S0034-4257(02)00074-3.

Nightingale, J., J. E. Nickeson, C. O. Justice, F. Baret, S. Garrigues, R. Wolfe, and E. Masuoka (2009), Global validation of EOS land products, lessons learned and future challenges: A MODIS case study, paper presented at the 33rd International Symposium on Remote Sensing of Environment: Sustaining the Millennium Development Goals, Stresa, Italy, May 4–8, 2009, pp. 4, http://landval.gsfc.nasa.gov/pdf/ISRSE_Nightingale.pdf.

Pauwels, V. R. N., N. E. C. Verhoest, G. J. M. De Lannoy, V. Guissard, C. Lucau, and P. Defourny (2007), Optimization of a coupled hydrology-crop growth model through the assimilation of observed soil moisture and leaf area index values using an ensemble Kalman filter, *Water Resour. Res.*, *43*(4), W04421, doi:10.1029/2006wr004942.

Pfeifer, M., A. Gonsamo, M. Disney, P. Pellikka, and R. Marchant (2012), Leaf area index for biomes of the Eastern Arc Mountains: Landsat and SPOT observations along precipitation and altitude gradients, *Remote Sens. Environ.*, *118*, 103–115, doi:10.1016/j.rse.2011.11.009.

Pinty, B., T. Lavergne, R. E. Dickinson, J. L. Widlowski, N. Gobron, and M. M. Verstraete (2006), Simplifying the interaction of land surfaces with

radiation for relating remote sensing products to climate models, *J. Geophys. Res.*, *111*, D02116, doi:10.1029/2005JD005952.

Pinty, B., M. Jung, T. Kaminski, T. Lavergne, M. Mund, S. Plummer, E. Thomas, and J. L. Widlowski (2011a), Evaluation of the JRC-TIP 0.01° products over a mid-latitude deciduous forest site, *Remote Sens. Environ.*, *115*(12), 3567–3581, doi:10.1016/j.rse.2011.08.018.

Pinty, B., I. Andredakis, M. Clerici, T. Kaminski, M. Taberner, M. M. Verstraete, N. Gobron, S. Plummer, and J. L. Widlowski (2011b), Exploiting the MODIS albedos with the Two-stream Inversion Package (JRC-TIP): 1. Effective leaf area index, vegetation, and soil properties, *J. Geophys. Res.*, *116*, D09105, doi:10.1029/2010jd015372.

Pinty, B., T. Lavergne, M. Voßbeck, T. Kaminski, O. Aussedat, R. Giering, N. Gobron, M. Taberner, M. M. Verstraete, and J. L. Widlowski (2007), Retrieving surface parameters for climate models from Moderate Resolution Imaging Spectroradiometer (MODIS)—Multiangle Imaging Spectroradiometer (MISR) albedo products, *J. Geophys. Res.*, *112*, D10116, doi:10.1029/2006jd008105.

Pisek, J., and J. M. Chen (2007), Comparison and validation of MODIS and VEGETATION global LAI products over four BigFoot sites in North America, *Remote Sens. Environ.*, *109*(1), 81–94, doi:10.1016/j.rse.2006.12.004.

Pisek, J., J. M. Chen, K. Alikas, and F. Deng (2010), Impacts of including forest understory brightness and foliage clumping information from multiangular measurements on leaf area index mapping over North America, *J. Geophys. Res.*, *115*, G03023, doi:10.1029/2009jg001138.

Plummer, S., O. Arino, M. Simon, and W. Steffen (2006), Establishing a Earth observation product service for the terrestrial carbon community: The globcarbon initiative, *Mitig. Adapt. Strat. Glob. Chang.*, *11*(1), 97–111, doi:10.1007/s11027-006-1012-8.

Rüdiger, C., C. Albergel, J.-F. Mahfouf, J.-C. Calvet, and J. P. Walker (2010), Evaluation of the observation operator Jacobian for leaf area index data assimilation with an extended Kalman filter, *J. Geophys. Res.*, *115*, D09111, doi:10.1029/2009jd012912.

Roujean, J. L., and R. Lacaze (2002), Global mapping of vegetation parameters from POLDER multiangular measurements for studies of surface-atmosphere interactions: A pragmatic method and its validation, *J. Geophys. Res.*, *107*(D12), 4150, doi:10.1029/2001JD000751.

Sabater, J. M., C. Rüdiger, J.-C. Calvet, N. Fritz, L. Jarlan, and Y. Kerr (2008), Joint assimilation of surface soil moisture and LAI observations into a land surface model, *Agr. Forest. Meteorol.*, *148*(8–9), 1362–1373, doi:10.1016/j.agrformet.2008.04.003.

Shabanov, N. V., et al. (2005), Analysis and optimization of the MODIS leaf area index algorithm retrievals over broadleaf forests, *IEEE Trans. Geosci. Remote Sens.*, *43*(8), 1855–1865, doi:10.1109/TGRS.2005.852477.

Sprintsin, M., A. Karnieli, P. Berliner, E. Rotenberg, D. Yakir, and S. Cohen (2009), Evaluating the performance of the MODIS Leaf Area Index (LAI) product over a Mediterranean dryland planted forest, *Int. J. Remote Sens.*, *30*(19), 5061–5069, doi:10.1080/01431160903032885.

Tang, H., K. Yu, X. Geng, Y. Zhao, K. Jiang, and S. Liang (2013), A time series method for cloud detection applied to MODIS surface reflectance images, *Int. J. Digital Earth*, In press.

Tian, Y., et al. (2004), Comparison of seasonal and spatial variations of leaf area index and fraction of absorbed photosynthetically active radiation from Moderate Resolution Imaging Spectroradiometer (MODIS) and Common Land Model, *J. Geophys. Res.*, *109*, D01103, doi:10.1029/2003JD003777.

Verger, A., F. Camacho, F. J. García-Haro, and J. Meliá (2009), Prototyping of Land-SAF leaf area index algorithm with VEGETATION and MODIS data over Europe, *Remote Sens. Environ.*, *113*(11), 2285–2297, doi:10.1016/j.rse.2009.06.009.

Weiss, M., F. Baret, S. Garrigues, and R. Lacaze (2007), LAI and fPAR CYCLOPES global products derived from VEGETATION. Part 2: Validation and comparison with MODIS collection 4 products, *Remote Sens. Environ.*, *110*(3), 317–331, doi:10.1016/j.rse.2007.03.001.

WMO (2011), Observational requirements from WMO and co-sponsored programmes and applications, http://www.wmo.int/pages/prog/sat/Databases.html#UserRequirements (Accessed on 31 March 2011).

Xiao, Z., S. Liang, J. Wang, P. Chen, X. Yin, L. Zhang, and J. Song (2013), Use of general regression neural networks for generating the GLASS leaf area index product from time-series MODIS surface reflectance, *IEEE Trans. Geosci. Remote Sens.*, doi:10.1109/TGRS.2013.2237780.

Yang, W., et al. (2006), MODIS leaf area index products: from validation to algorithm improvement, *IEEE Trans. Geosci. Remote Sens.*, *44*(7), 1885–1898, doi:10.1109/TGRS.2006.871215.